CHAPTER 3

RESULTS AND DISSCUSSION

The results of this study were divided into 6 parts as the followings:

Part 1 : Construction of GFP, Tat/GFP, VP/GFP and VP/Tat/GFP fusion protein expression plasmid

Part 2 : Expression and purification of GFP, Tat/GFP, VP/GFP and VP/Tat/GFP fusion protein

Part 3 : Cellular uptake of GFP, Tat/GFP, VP/GFP and VP/Tat/GFP fusion protein

Part 4 : Cellular uptake efficiency enhancement strategy

Part 5 : *In vitro* calcitonin activity of Tat/sCT, VP/sCT and VP/Tat/sCT mixtures

Part 6 : *In vivo* calcitonin activity of Tat/sCT, VP/sCT and VP/Tat/sCT mixtures

Part 1 : Construction of GFP, Tat/GFP, VP/GFP and VP/Tat/GFP fusion protein expression plasmid

1.1. Amplification of genes encoding GFP, Tat/GFP, VP/GFP and VP/Tat/GFP fusion protein

The effect of N-terminal and C-terminal fusion on cellular uptake efficiency was evaluated using Tat/GFP fusion protein. N-terminal Tat-GFP fusion protein gave higher cellular uptake than C-terminal GFP-Tat fusion protein. Thus, only N-terminal fusion was produced for VP/GFP fusion protein (VP-GFP). Tat-GFP-VP was also produced to determine whether the fusion of both Tat and VP could provide the synergistic effect or not. PCR products of GFP, GFP-Tat, Tat-GFP, VP-GFP and Tat-

GFP-VP were shown in Figure 16-17. The sizes of all PCR products were in line with the actual size calculated from amino acid number.

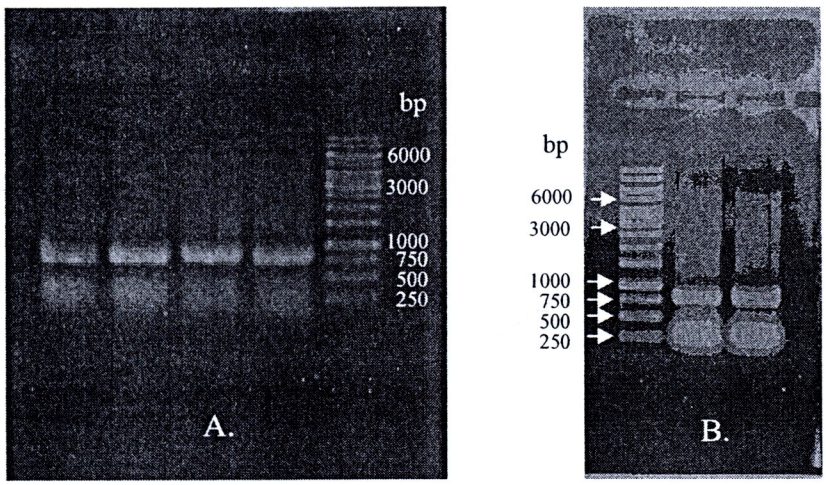

Figure 16 (A) PCR product of GFP (lane 1 and 2; approx. size = 737 bp), PCR product of GFP-Tat (lane 3 and 4; approx. size = 764 bp) and 1 kb DNA ladder. (B) 1 kb DNA ladder (lane 1), PCR product of Tat-GFP (lane 2 and 3; approx. size = 764 bp)

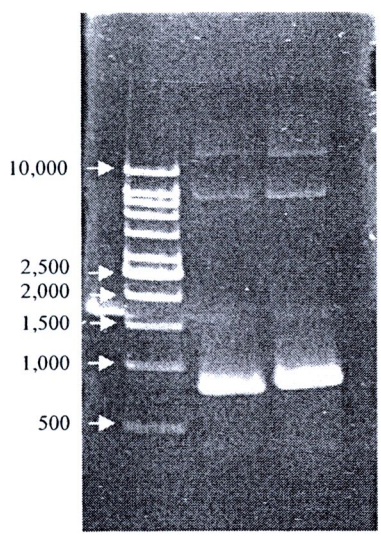

Figure 17 PCR product of VP-GFP (lane 2; approx. size = 788 bp) and Tat-GFP-VP (lane 3; approx. size = 815 bp) comparing with VC 1 kb DNA ladder (lane 1)

1.2. Construction of GFP, Tat/GFP, VP/GFP and VP/Tat/GFP fusion protein expression vectors

The pET28a(+) vector and PCR fragments were prepared for expression vector construction by digest with *Nhe*I and *Bam*HI restriction enzyme. Agarose electrophoresis of pET28a(+) and all PCR fragments after digested with *Nhe*I and *Bam*HI were shown in Figure 18-19. The digested fragments were ligated into linearized pET28a(+) between *Nhe*I and *Bam*HI restriction site. The ligation products were resolved by agarose gel electrophoresis and the result was demonstrated in Figure 20-21.

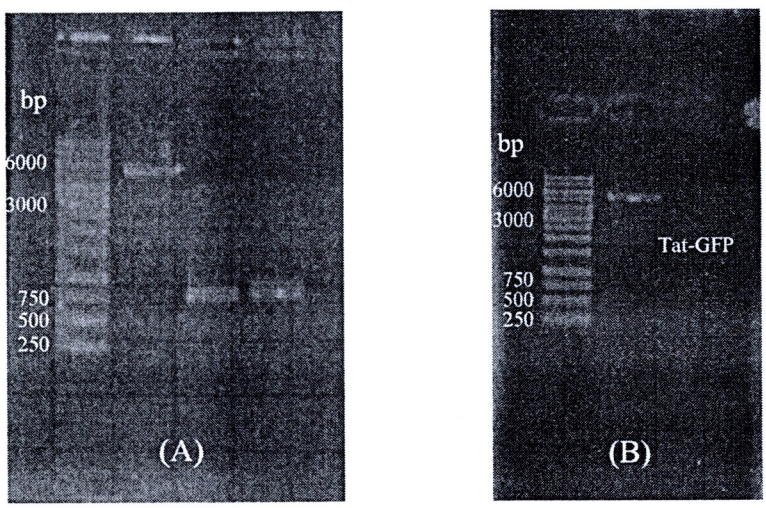

Figure 18 Agarose electrophoresis of (A) 1 kb DNA ladder (lane 1), linearized pET28a(+) (lane 2), digested GFP (lane 3) and digested GFP-Tat (lane 4) (B) 1 kb DNA ladder (lane 1), linearized pET28a(+) (lane 2) and digested Tat-GFP (lane 3)

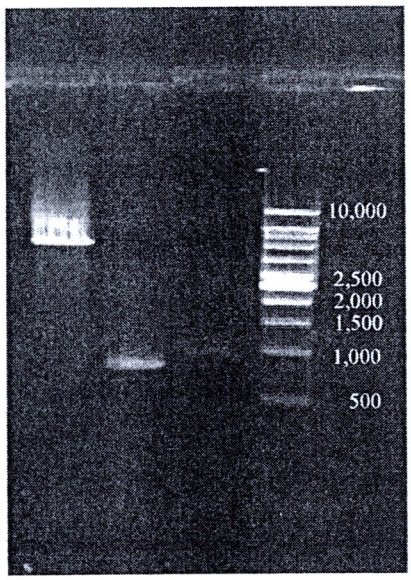

Figure 19 Agarose electrophoresis of linearized pET28a(+) (lane 1), digested VP-GFP (lane 2) and digested Tat-GFP-VP (lane 3) and 1 kb DNA ladder (lane 4)

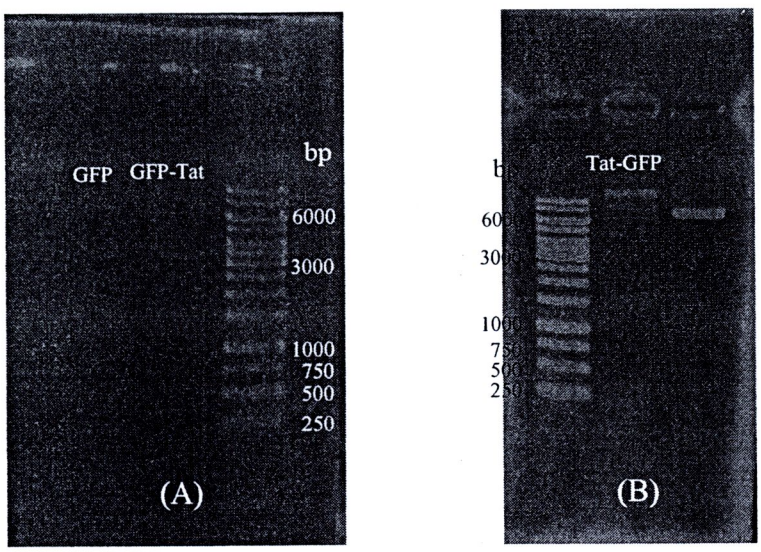

Figure 20 Agarose electrophoresis of ligation products (A) pET28a(+)GFP (lane 1; 6059 bp), pET28a(+)GFP-Tat (lane 2; 6086 bp) and 1 kb DNA ladder (B) 1 kb DNA ladder (lane 1), pET28a(+)Tat-GFP (lane 2; 6086 bp) and pET28a(+) without insertion (lane 3; 5369 bp)

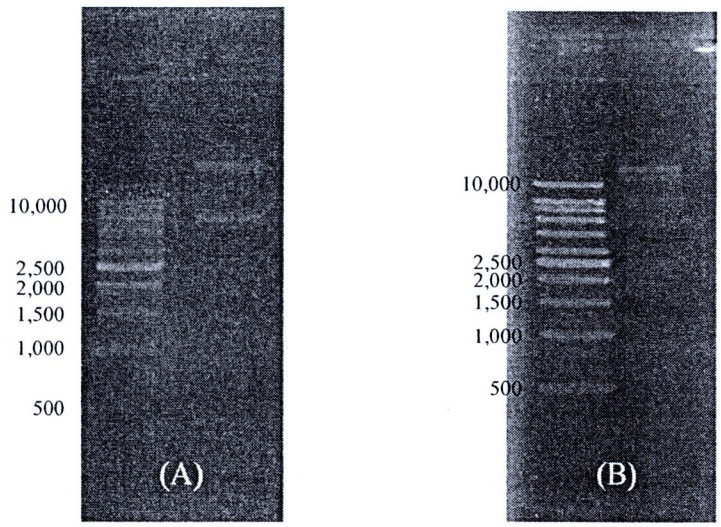

Figure 21 Agarose electrophoresis of ligation products (A) VC 1 kb DNA ladder (lane 1) and pET28a(+)VP-GFP (lane 2; 6110 bp) (B) VC 1 kb DNA ladder (lane 1) and pET28a(+)Tat-GFP-VP (lane 2; 6137 bp)

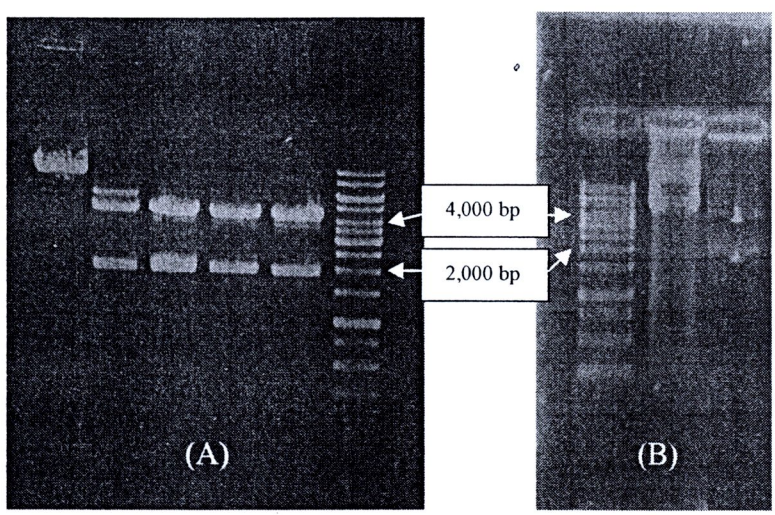

Figure 22 Agarose electrophoresis of (A) pET28a(+) digested with HpaI (lane 1), pET28a(+)GFP digested with HpaI (lane 2), pET28a(+)GFP-Tat digested with HpaI (lane 3), pET28a(+)Tat-GFP digested with HpaI (lane 4), pET28a(+)VP-GFP digested with HpaI (lane 5) and 1 kb DNA ladder (lane 6) (B) pET28a(+) digested with HpaI (lane 1) and pET28a(+)Tat-GFP-VP digested with HpaI (lane 2)

Part 2 : Expression and purification of GFP, Tat/GFP, VP-GFP and VP/Tat/GFP fusion protein

2.1. Transformation of expression vectors and colony screening

After transformation, the transformant was selected using LB medium containing 30 μg/ml of kanamycin. The selected transformed *E. coli* DH5α was propagated for plasmid purification and confirmed the insertion by *Hpa*I digesting and sequencing. With the fragment carrying GFP sequence insert in the correct location and orientation in pET28a(+), digestion with *Hpa*I would produce two band of ~4 kb and ~2 kb. *Hpa*I digestion of non-recombinant pET28a(+) gave only one band at vector size (~5.3 kb) (Figure 22). The purified plasmid was sequenced using the same primers as used in PCR. The obtained nucleotide sequences were analyzed by the alignment tool on National Center for Biotechnology Information (NCBI) website. *E. coli* transformed with plasmid encoding GFP sequence could be detected under fluorescent microscope as shown in Figure 23.

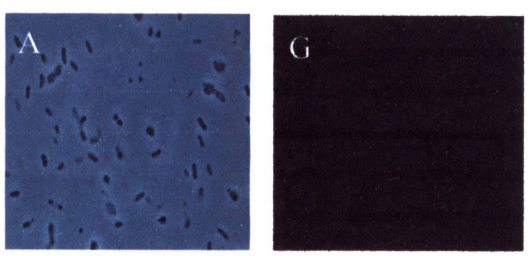

Figure 23 *E. coli* DH5α transformed with pET28a(+) (A and G), pET28a(+)GFP (B and H), pET28a(+)GFP-Tat (C and I), pET28a(+)Tat-GFP (D and J), pET28a(+) VP-GFP (E and K) and pET28a(+)Tat-GFP-VP (F and L). A-F and G-L were captured under transmission light and fluorescent filter, respectively.

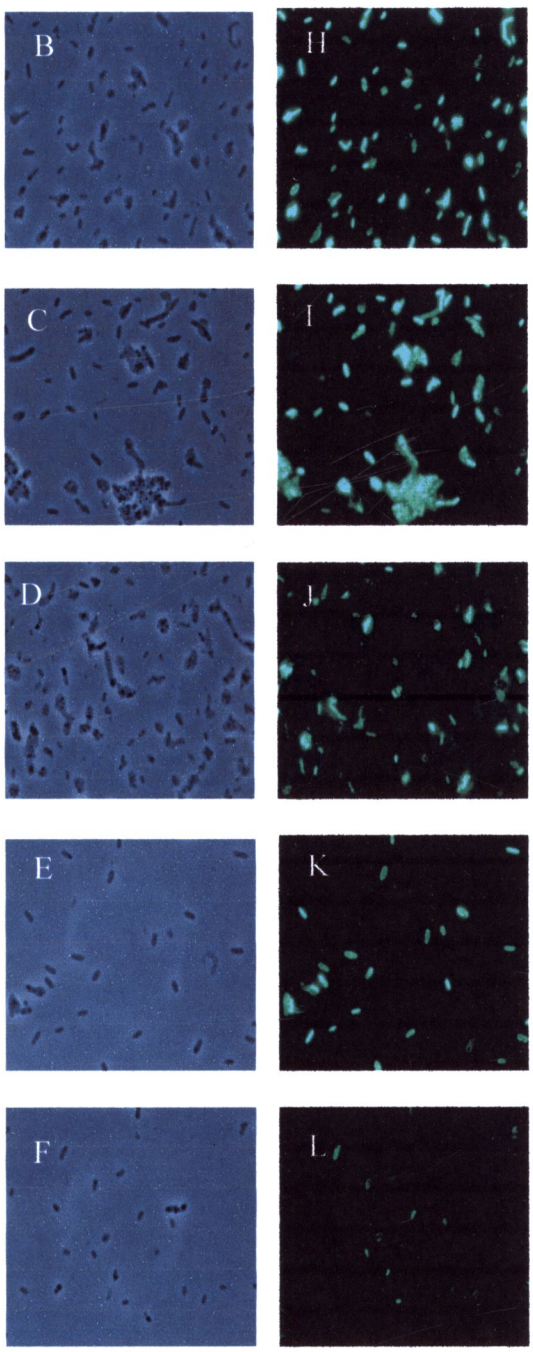

Figure 23 *E. coli* DH5α transformed with pET28a(+) (A and G), pET28a(+)GFP (B and H), pET28a(+)GFP-Tat (C and I), pET28a(+)Tat-GFP (D and J), pET28a(+) VP-GFP (E and K) and pET28a(+)Tat-GFP-VP (F and L). A-F and G-L were captured under transmission light and fluorescent filter, respectively (continued).

THE NATIONAL RESEARCH COUNCIL OF THAILAND
RESEARCH LIBRARY

2.2. Protein expression and purification

2.2.1. Target protein verification for expression level and solubility

E. coli BL21 (DE3) transformed with pET28a(+)GFP and pET28a(+)GFP-Tat were used to verify target protein expression level and solubility. Protein expression was analyzed in 3 fractions: total protein fraction (TCP), soluble cytoplasmic fraction and insoluble cytoplasmic fraction. Mostly of the target protein was found in insoluble cytoplasmic fraction (Figure 24). Thus, the sonication step was necessary to resuspend the pellet and induced the releasing of trapped proteins. The effect of IPTG concentration and incubation time on the protein expression level was evaluated. The result showed that no significant difference of protein expression level could be observed when IPTG concentration increased from 0.1 to 1 mM (Figure 25). In contrast, the protein expression level was increased when the incubation time increased and reached the maximum within 3 hr (Figure 26). Hence, the expression condition by IPTG induction at final concentration of 0.1 mM for 3 hr was applied for all fusion protein.

2.3. Analysis of purified proteins

After purification process, all target proteins were resolved in SDS-PAGE. The fusion proteins were purified by affinity chromatography using a metal-chelating matrix, and the purified fusion proteins were found to be nearly homogeneous and > 90% pure, as determined by SDS-PAGE analysis with Coomassie Brilliant blue staining. The GFP protein migrated at the expected size. In the presence of Tat/VP moiety, the higher molecular mass than the control GFP were observed (Figure 27).

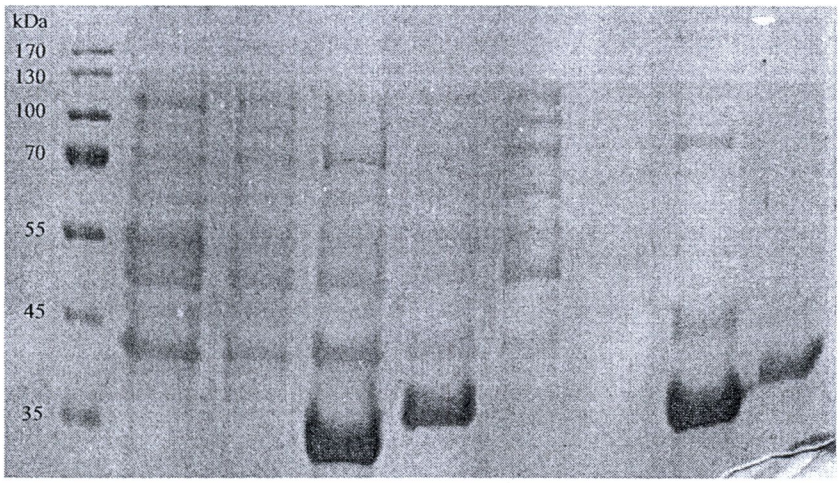

Figure 24 Sodium dodecyl sulfate polyacrylamide gel electrophoresis (SDS-PAGE) analysis of the expressed proteins from non-transformed *E. coli* BL21 (DE3) (lane 2), *E: coli* BL21 (DE3) transformed with pET28a(+) (lane 3), *E. coli* BL21 (DE3) transformed with pET28a(+)GFP (lane 4, 6 and 8) and *E. coli* BL21 (DE3) transformed with pET28a(+)GFP-Tat (lane 5, 7 and 9). Lanes 2-5 were TCP fraction. Lanes 6-7 were soluble cytoplasmic fractions. Lanes 8-9 were insoluble cytoplasmic fractions. Pre-stained protein marker (Fermentas, St. Leon-Rot, Germany) was shown in lane 1.

The purified GFP, GFP-Tat and Tat-GFP were further recognized by western blot analysis using antibody against penta-Histisine residue as shown in Figure 28. Fluorescence intensity was compared between each construct by Multimode Reader (Beckman, California, USA). Tat residue could reduce the fluorescent intensity of GFP of about 50-60% and in the presence of VP moiety, the fluorescent intensity was only 20% of GFP (Figure 29).

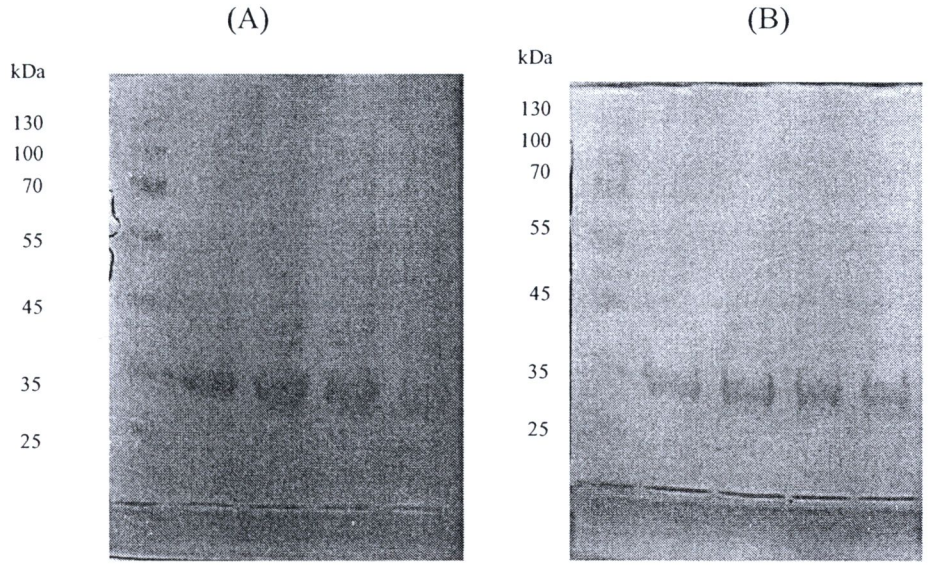

Figure 25 SDS-PAGE analysis of GFP (A) and GFP-Tat (B) expression after IPTG induction at final concentration 0.1 mM (lane 2), 0.2 mM (lane 3), 0.4 mM (lane 4) and 1 mM (lane 5) for 3 hr. Lane 1 was Pre-stained protein marker.

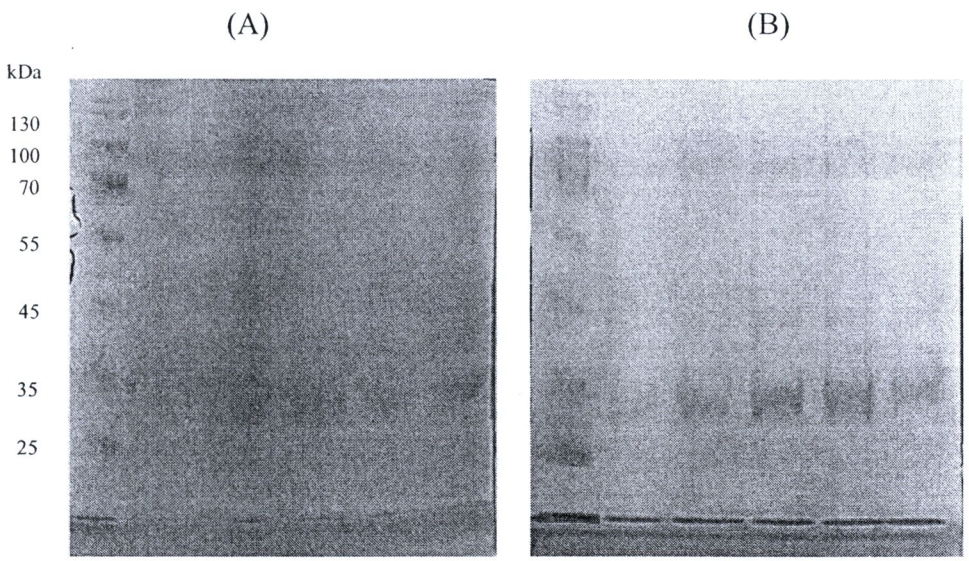

Figure 26 SDS-PAGE analysis of GFP (A) and GFP-Tat (B) expression after IPTG induction at final concentration 0.1 mM for 1 hr (lane 2), 2 hr (lane 3), 3 hr (lane 4), 4 hr (lane 5) and 5 hr (lane 6). Lane 1 was Pre-stained protein marker.

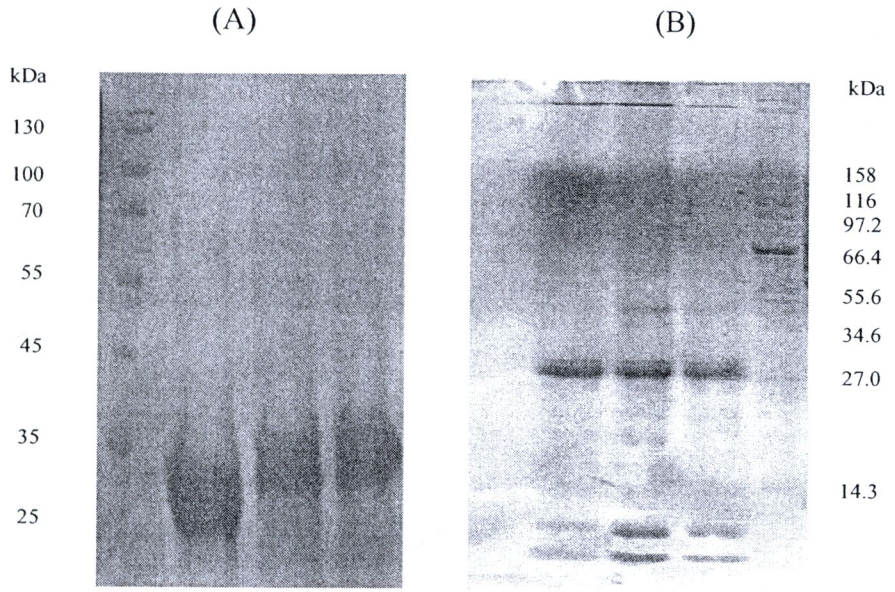

Figure 27 (A) Analysis of the purified GFP (lane2; ~28 kDa), GFP-Tat (lane 3; ~30 kDa) and Tat-GFP (lane 4; ~30 kDa) by 12% SDS-PAGE (B) Purified Tat-GFP (lane 1; ~30 kDa), VP-GFP (lane 2; ~30 kDa) and Tat-GFP-VP (lane 3; ~32 kDa) resolved in SDS-PAGE.

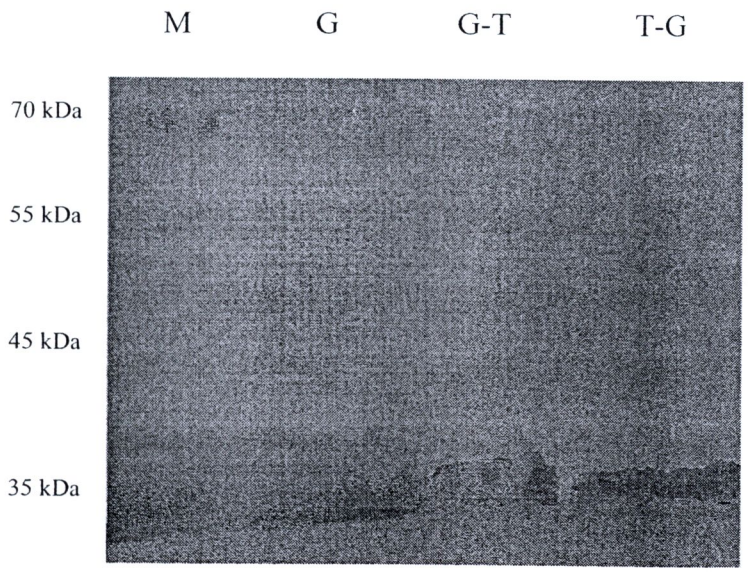

Figure 28 Western blot analysis using anti-penta-His-HRP conjugate antibody. M : molecular weight markers, G : GFP, G-T : GFP-Tat fusion protein, T-G : Tat-GFP fusion protein

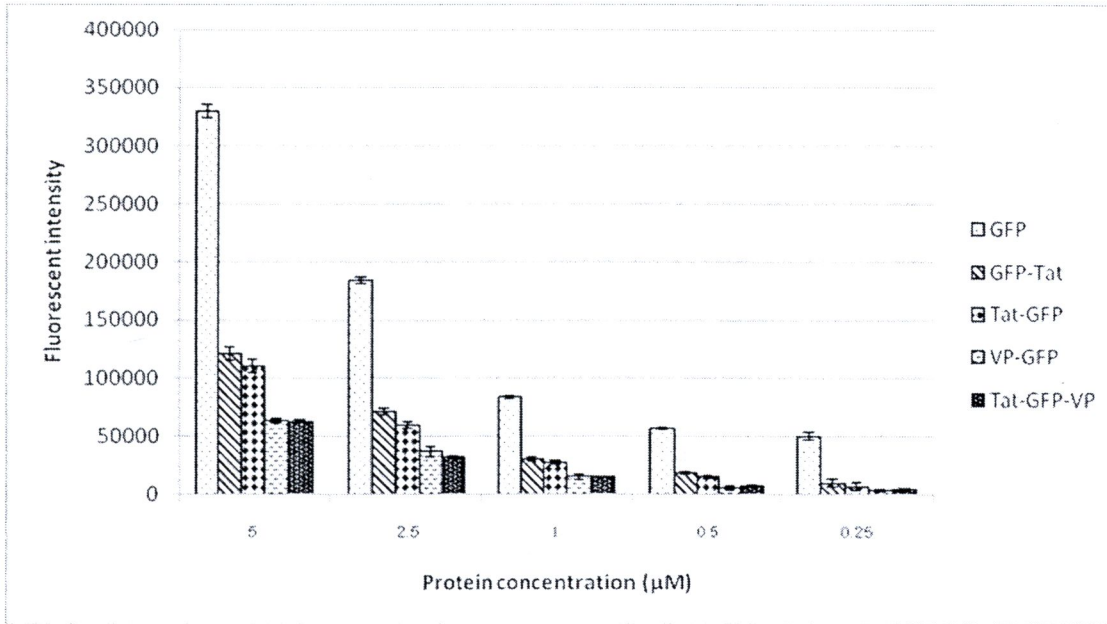

Figure 29 Fluorescent intensity at various concentrations of GFP, GFP-Tat, Tat-GFP, VP-GFP and Tat-GFP-VP fusion protein

Part 3 : Cellular uptake of GFP, Tat/GFP, VP/GFP and VP/Tat/GFP fusion protein

Cellular uptake study was performed in 2 types of gastro-intestinal (GI)-lining cell lines, KB (human mouth epidermal carcinoma) and HT-29 (human colon adenocarcinoma) cells. Uptake efficiency of Tat-GFP and GFP-Tat fusion protein were compared to evaluate the effect of N-terminal or C-terminal fusion on the enhancement of GFP uptake. The higher uptake of Tat-GFP and GFP-Tat fusion proteins than GFP in the both cell lines was observed (Figure 30). This might be due to the effects of Tat which enhanced the cellular internalization (Lindsay, 2002). Tat-GFP, the N-terminal fusion protein of GFP gave the highest uptake efficiency of about 2-3 times higher than GFP control due to the effects from the protein folding resulting from the different type of peptide terminal (Schelhaas et al., 2007).

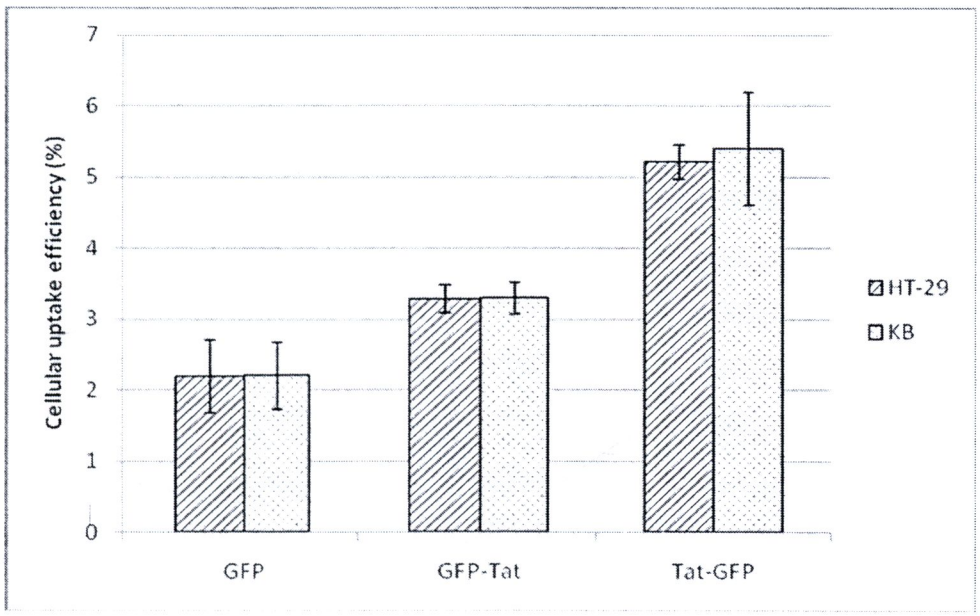

Figure 30 Cellular uptake efficiency represented as percentage of protein detected in HT-29 and KB cells after 1 hour incubation with GFP or Tat/GFP fusion proteins at 1 μM.

In addition, cellular uptake of both GFP-Tat and Tat-GFP were concentration dependent as shown in Figure 31. All fusion proteins were rapidly uptake and reached the maximum within 1 hr (Figure 32). The rapid internalization of Tat-streptavidin within 5 min has also been reported (Rinne et al., 2007). Thus, the 1 hr incubation time was used for further study.

The results from CLSM visualization as shown in Figure 33 demonstrated the translocation of GFP fluorescent signal in all samples in cytoplasm and nucleus, but not adsorbed at the cell membrane. Thus, the obtained uptake efficiency data calculated from the fluorescent intensity of the lysed cells could represent the amount of protein translocated into the cells, not from the adsorption to the cell membrane. The fluorescent intensity determination was used to evaluate the uptake efficiency for further experiments.

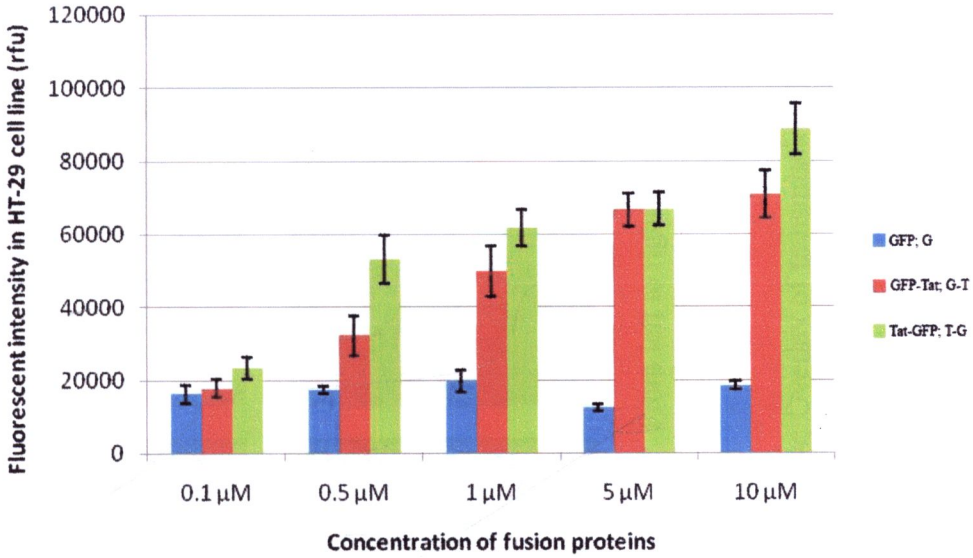

Figure 31 Cellular uptake efficiency of GFP and Tat/GFP fusion proteins in HT-29 cell lines as fluorescent intensity units (rfu) after incubation for 1 hour with various concentrations of GFP, GFP-Tat and Tat-GFP fusion proteins.

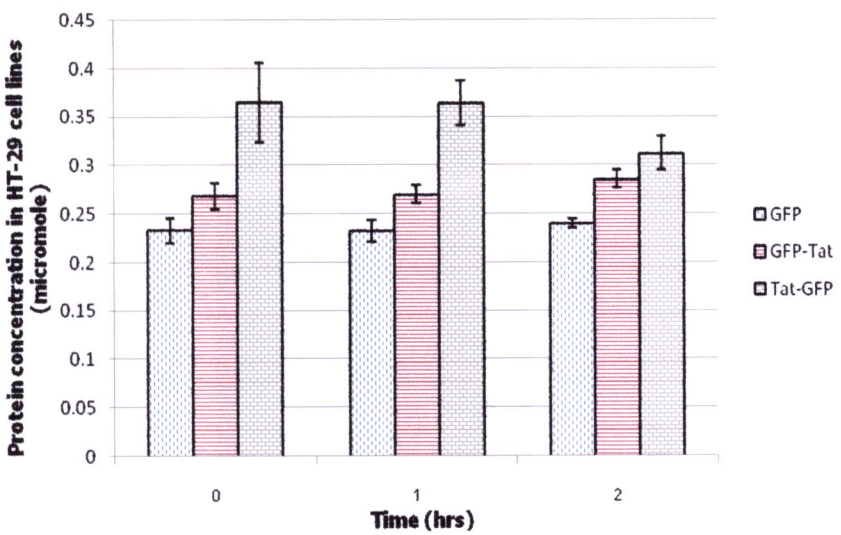

Figure 32 The effect of incubation time on cellular uptake of GFP and Tat/GFP fusion proteins in HT-29 cell lines. The concentration of all samples was 1 μM.

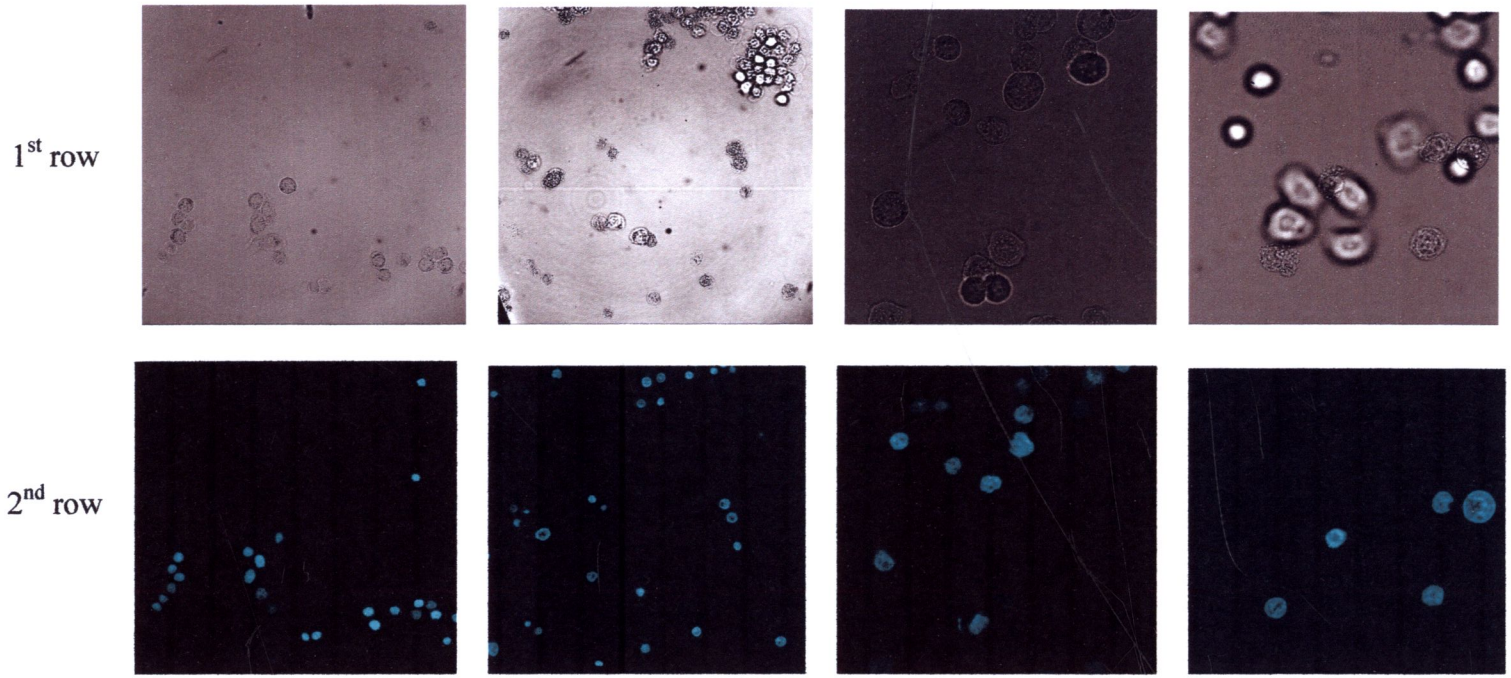

Figure 33 CLSM pattern from uptake study of N-terminal 6XHis GFP, GFP-Tat and Tat-GFP. From left to right; Control, GFP, GFP-Tat and Tat-GFP

First row: Transmission view; Second row: DAPI staining; Third row: GFP filter; Fourth row; Overlay of transmission, DAPI and GFP filter (White arrow indicate the green fluorescent area)

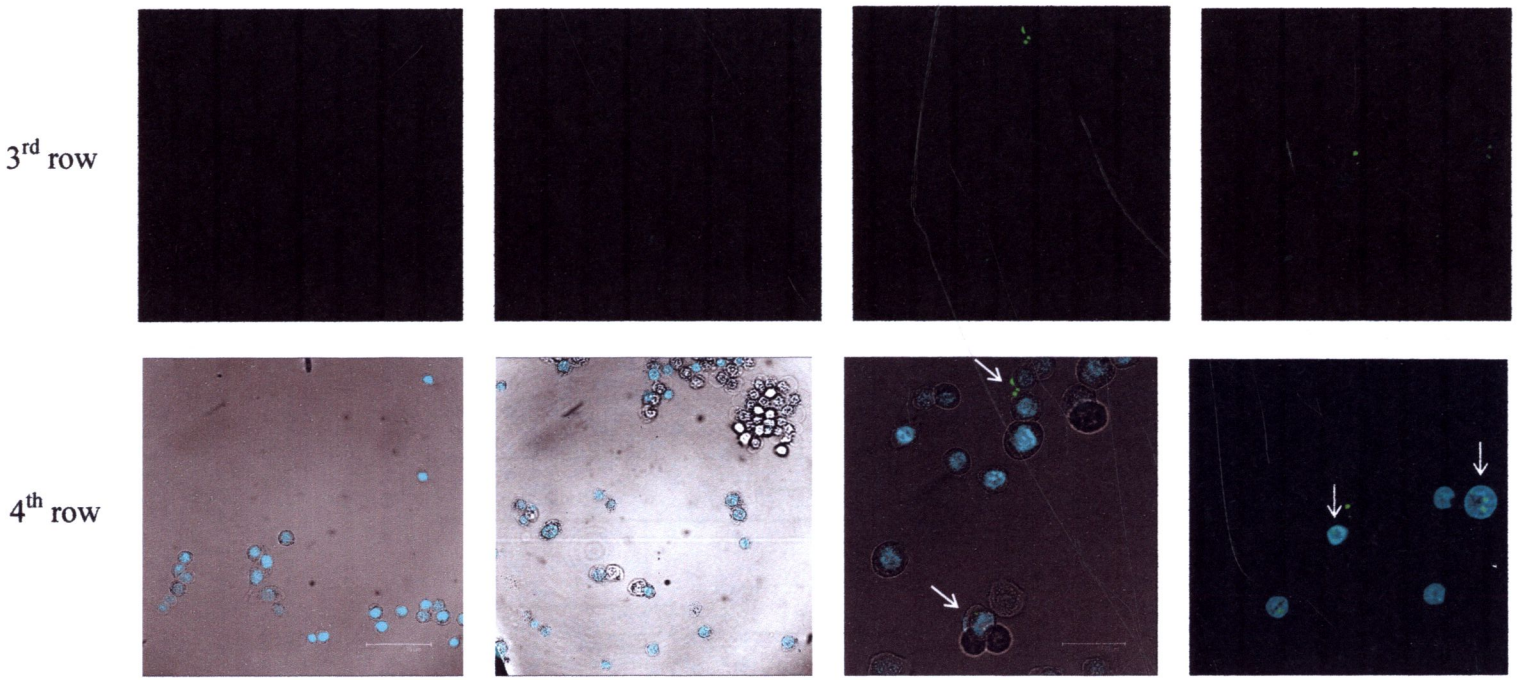

Figure 33 CLSM pattern from uptake study of N-terminal 6XHis GFP, GFP-Tat and Tat-GFP. From left to right; Control, GFP, GFP-Tat and Tat-GFP (continued)

First row: Transmission view; Second row: DAPI staining; Third row: GFP filter; Fourth row; Overlay of transmission, DAPI and GFP filter (White arrow indicate the green fluorescent area)

Cellular uptake efficiency of VP-GFP and Tat-GFP-VP fusion protein was demonstrated in Figure 34. N-terminal fusion of VP residue could also enhance the uptake of GFP into HT-29 and KB cells but the uptake efficiency was still lower than Tat-GFP fusion protein. Moreover, cellular uptake of Tat-GFP-VP fusion protein was lower than either Tat-GFP or VP-GFP indicated that no synergistic effect of Tat and VP on the enhancement of GFP uptake. Since Tat-GFP fusion protein gave superior cellular uptake than other fusion protein, Tat-GFP was selected for **Part 4 : Cellular uptake efficiency enhancement strategy**.

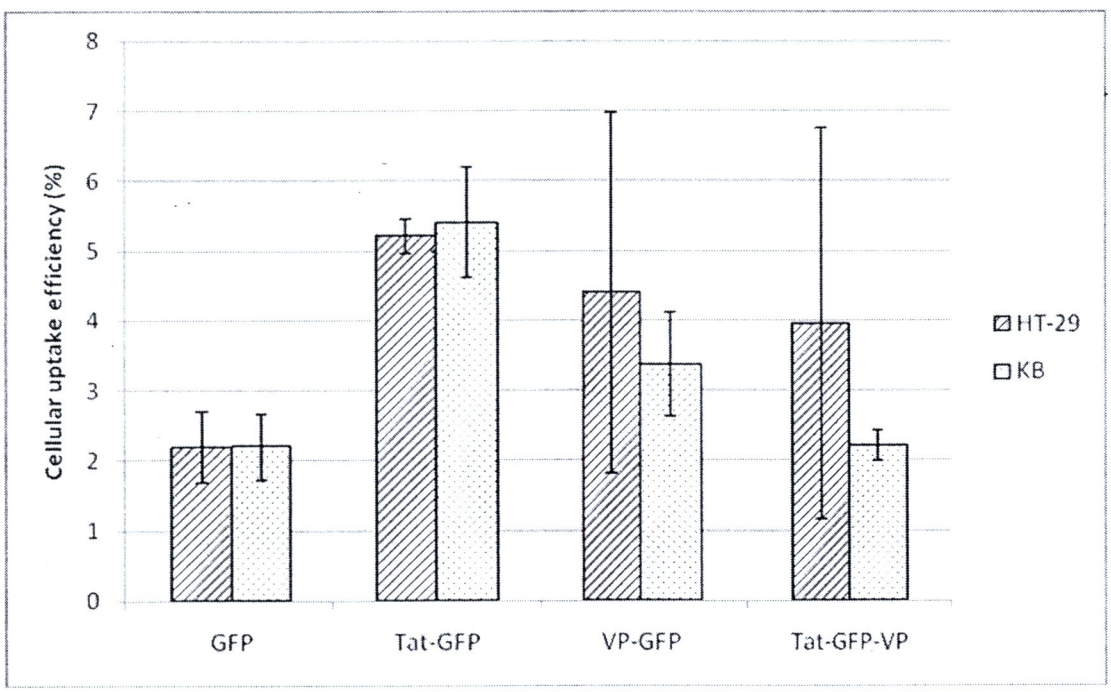

Figure 34 Cellular uptake efficiency represented as percentage of protein detected in HT-29 and KB cells after 1 hour incubation with GFP or Tat/VP/GFP fusion proteins at 1 μM.

Part 4 : Cellular uptake efficiency enhancement strategy

Even if Tat-GFP demonstrated 2-3 times higher cellular uptake efficiency than GFP, the uptake efficiency was still lower than 6% which might not enough for the application as drug delivery system. Thus, other strategies were needed. Two different methods, entrapment in nanovesicles and co-incubation strategy were evaluated for the efficiency in cellular uptake enhancement.

4.1. Entrapment in nanovesicles

4.1.1. Preparation and physical properties determination of nanovesicular formulations (liposomes/niosomes)

A. Mean particle sizes and zeta potential

After lyophilization, all empty nanovesicular formulations (liposomes/niosomes) were white powder. The vesicular size and zeta potential of non-elastic or elastic nanovesicles with and without Tat-GFP were shown in Table 6. The non-elastic niosomes (50.96±10.93 to 195.78±59.47 nm) showed larger vesicular sizes than the non-elastic liposomes (50.77±0.89 to 88.67±3.66 nm). This might be due to the closer packing of liposomes from the smaller size polar head group of DPPC than Tween 61 of niosomes (Taylor et al., 2007; Manosroi et al., 2010). However, the elastic liposomes (172.71±83.17 to 777.83±13.95 nm) showed slightly larger vesicular size than the elastic niosomes (203±49.07 to 690.73±8.78 nm). This may be due to the synergistic effect of ethanol and Tween 61 which acted as an edge activator resulting in the more flexibility of niosomes than liposomes which contained the more rigid phospholipid molecules. Therefore, the smaller vesicular size of niosomes were obtained (Maghraby et al., 2004). Most loaded nanovesicles showed larger vesicular size than the non-loaded nanovesicles. The elastic nanovesicles showed larger vesicular size than its corresponding non-elastic nanovesicles. This

agreed with the report of the dramatically increase in the average size of vesicles when ethanol concentration in the formulation was in the range of 20% to 30% (Verma and Fahr, 2004). The zeta potential of both Tat-GFP loaded and non-loaded nanovesicles were in the range of (-) 17.3±3.33 to 36.6±2.95 mV. The zeta-potential values of the elastic vesicles were more negative than the non-elastic vesicles, owing to the presence of ethanol in the elastic vesicles which may impart negative charges from the hydroxyl group of ethanol (Choi and Malbach, 2005). All neutral and anionic nanovesicles showed negative zeta potential values due to the negative nature of their composition, including cholesterol and DP, while the cationic vesicles gave positive zeta potential values from the cationic lipid, DDAB. In addition, flocculation was observed in neutral niosomes and liposomes after 24 hr owing to the lack of repulsive force between the vesicles thereby resulting in aggregation (Kayes, 1977).

B. Entrapment efficiency of Tat-GFP loaded in nanovesicles

Entrapment efficiencies of Tat-GFP loaded in various nanovesicles were in the range of 7.93 to 100% (Table 7). For niosomes, elastic cationic niosomes showed the highest entrapment efficiency of 100%. This might be due to the effect of charge interaction between the positive charge of the vesicles and the negative charge of the fusion protein, Tat-GFP at pH 7.0. Usually, most hydrophilic compounds can be entrapped in the vesicles of not mot more than 10-20%. This high entrapment efficiency was due to the entrapment of Tat-GFP both inside the aqueous phase and adsorbed on the surface of the vesicular membrane by an electrostatic interaction (McLaughlin et al., 1971; Manosroi et al., 2010a).

Table 6 Vesicular sizes (nm) and zeta potential (mV) of the blank and Tat-GFP loaded nanovesicles

Type of nanovesicles		Size (nm)		Zeta potential (mV)	
		Blank nanovesicles	*Tat-GFP loaded nanovesicles*	*Blank nanovesicles*	*Tat-GFP loaded nanovesicles*
Niosomes	Non-elastic neutral niosome*	195.78±59.47	107.48±16.72	-10.8±0.76	-8.26±0.96
	Elastic neutral niosome*	203±49.07	374.63±17.24	-17.3±3.33	-15.1±4.67
	Non-elastic cationic niosome*	81.3±14.65	117.33±22.94	-5.27±2.44	-5.2±1.51
	Elastic cationic niosome	384.5±29.3	328.37±27.39	-7.92±1.54	-7.9±1.09
	Non-elastic anionic niosome	50.96±10.93	182.97±14.59	-4.73±0.94	-2.79±1.22
	Elastic anionic niosome	341.2±64.35	690.73±8.78	-9.07±0.28	-8.49±0.84
Liposomes	Non-elastic neutral liposome*	69.46±33.21	76.34±8.82	1.25±0.59	-2.55±0.71
	Elastic neutral liposome*	222.13±18.35	172.71±83.17	-13.5±2.25	-12.7±3.16
	Non-elastic cationic liposome	57.11±4.6	88.67±3.66	36.6±2.95	32.6±2.19
	Elastic cationic liposome	551.8±68.48	433.23±102.35	21.4±2.84	24.5±3.68
	Non-elastic anionic liposome	50.77±0.89	68.6±1.56	-9.03±2.76	-2.72±0.96
	Elastic anionic liposome	392.97±4.94	777.83±13.95	-16.9±0.77	-14.6±1.05

* Flocculation was observed

The highest entrapment efficiency for liposomes formulations was found in the elastic cationic liposomes of at only 38.28±13.77%. Lower entrapment efficiency of liposomes in comparing to niosomes might be due to the mechanical instability of liposomes which may cause the leakage of the loaded substances (Axthelm, 2008). The elastic nanovesicular formulations of both liposomes and niosomes gave higher entrapment efficiency than the non-elastic nanovesicles. This might be due to the increase solubility of Tat-GFP by ethanol that may facilitate the loading (Lópes-Pinto and González-Rodriguez, 2005). Both elastic and non-elastic niosomes showed higher entrapment efficiency than liposomal formulations due to the larger structure of the polar head group of Tween 61 in comparing to those of DPPC resulting in the larger inner aqueous core and the aqueous space between the bilayers of the vesicles, thereby facilitating the entrapment efficiency of Tat-GFP which was a water-soluble substance. Also, in niosomes, Tween 61 which is a non-ionic surfactant can act as a solubilizer better than phospholipids in liposomes, hence, the entrapment efficiency of Tat-GFP in niosomes can be higher than in liposomes (Manosroi et al., 2010a).

Table 7 Entrapment efficiency of Tat-GFP fusion protein in various nanovesicular formulations

Tat-GFP loaded in	**Entrapment efficiency (%)**
Non-elastic neutral niosomes	53.75±6.29
Elastic neutral niosomes	33.91±5.88
Non-elastic cationic niosomes	35.81±1.46
Elastic cationic niosomes	100±0.00

Table 7 Entrapment efficiency of Tat-GFP fusion protein in various nanovesicular formulations (continued)

Tat-GFP loaded in	Entrapment efficiency (%)
Non-elastic anionic niosomes	32.09±0.09
Elastic anionic niosomes	32.76±5.85
Non-elastic neutral liposomes	21.15±9.95
Elastic neutral liposomes	20.81±10.94
Non-elastic cationic liposomes	15.24±13.47
Elastic cationic liposomes	38.28±13.57
Non-elastic anionic liposomes	7.93±3.34
Elastic anionic liposomes	35.55±18.72

C. Deformability index (DI) determination

Most blank elastic nanovesicles indicated higher elasticity with higher DI values than the non-elastic nanovesicles with the maximum DI of 12.69±1.43 in elastic neutral niosomes which was 1.38 folds of the non-elastic neutral niosomes (Table 8). Ethanol existing in the vesicles might interact with the polar head-group of the phospholipid or surfactant molecules, resulting in the reduction of melting point, thereby increasing the fluidity of the vesicles (Touitou et al., 2000; Manosroi et al., 2009). However, niosomes showed higher DI values than the liposomal formulations due to the presence of Tween 61, a polysorbate surfactant, which is an edge activator that may also confer elastic properties to the vesicles (Maghraby et al., 2004).

THE NATIONAL RESEARCH COUNCIL OF THAILAND RESEARCH LIBRARY

Table 8 Deformability index (DI) and the DI ratios of the blank nanovesicles

Type of vesicles		Deformability index (DI)	The DI ratio between elastic and the corresponding non-elastic nanovesicles
Niosomes	Non-elastic neutral niosome*	9.19±0.67	-
	Elastic neutral niosome*	12.69±1.43	1.38
	Non-elastic cationic niosome*	2.37±0.05	-
	Elastic cationic niosome	3.58±0.72	1.51
	Non-elastic anionic niosome	5.81±2.91	-
	Elastic anionic niosome	10.92±0.02	1.88
Liposomes	Non-elastic neutral liposome*	1.62±0.55	-
	Elastic neutral liposome*	5.04±1.96	3.11
	Non-elastic cationic liposome	2.18±0.18	-
	Elastic cationic liposome	2.95±1.13	1.35
	Non-elastic anionic liposome	0.49±0.42	-
	Elastic anionic liposome	0.12±0.03	0.24

* Flocculation was observed

4.1.2. Cellular uptake and cytotoxicity of Tat-GFP loaded nanovesicles

Cellular uptake efficiency of Tat-GFP loaded in various nanovesicular formulations was shown in Table 9. Tat-GFP loaded in elastic anionic niosomes which their corresponding blank vesicles gave the high DI of 10.92±0.02 showed the highest uptake of 14.62±0.07% and 15.32±0.96% in HT-29 and KB cells which was 2.81 and 2.84 folds of free Tat-GFP uptake in each cell lines. This might be from not

only the elasticity of the vesicles, but also the physical characteristics and compositions of the vesicles as well. The ethanol in the vesicles may damage the hydrophobic core of the membrane resulting in the increasing of membrane permeability (Mizoguchi and Hara, 1998), thereby increasing the cellular uptake. However, elastic neutral niosomes which their corresponding blank vesicles showed the highest DI value (12.69±1.43) gave lower uptake efficiency. This may be due to the low entrapment efficiency (33.91±5.88%) of this formulation. All liposomal formulations which demonstrated low entrapment efficiency also demonstrated lower cellular uptake in comparing to the corresponding charged niosomes. When loaded in non-elastic niosomes and liposomes, Tat-GFP gave the cellular uptake efficiency in the range of 1.09 to 2.59 folds higher than GFP, but still lower than the non-loaded Tat-GFP protein. This has indicated the cellular uptake enhancement of GFP by fusion with Tat and loaded in elastic, but not in non-elastic vesicles. Although the entrapment efficiency of Tat-GFP in all elastic vesicles (except cationic elastic niosomes) were less than 40%, the enhancement of Tat-GFP uptake when loaded in elastic vesicles were still superior over the free Tat-GFP of 1.41 to 2.85 folds.

For cytotoxicity assay, the Tat-GFP fusion proteins gave cell viability at 62.46±3.11%. Tat-GFP loaded in non-elastic niosomes and liposomes showed less cytotoxicity than the free Tat-GFP and Tat-GFP loaded in elastic vesicles. Tat-GFP loaded in non-elastic vesicles gave cell viability at 72.90±21.86 to 97.71±1.44%. This agreed with the previous report which indicated that the decrease toxicity of the substances was observed when loaded in nanovesicles (Biju et al., 2006). However, Tat-GFP loaded in elastic anionic niosomes which showed the highest cellular uptake demonstrated obviously cytotoxicity effect with cell viability of only 37.29±0.67%

and 62.48±5.58 in HT-29 and KB cells. Tat-GFP loaded in all elastic vesicles gave higher cytotoxicity than Tat-GFP loaded in all non-elastic vesicles and the free Tat-GFP especially in HT-29 cells. This was due to the ethanol composition in the elastic vesicles which could increase cell toxicity by causing cell membrane leakage (Mizoguchi and Hara, 1998).

Table 9 Cellular uptake of Tat-GFP fusion protein and cell viability of HT-29 cells after incubated with various nanovesicular formulations

Tat-GFP loaded in	**Cellular Uptake (%)***		**Cell viability (%)**	
	HT-29	**KB**	**HT-29**	**KB**
Non-elastic neutral niosomes	2.84±0.16	5.70±0.11	96.71±1.17	96.66±14.86
Elastic neutral niosomes	7.35±0.03	8.53±0.08	35.73±2.47	89.56±1.15
Non-elastic cationic niosomes	2.38±0.35	11.72±0.12	92.08±1.88	84.73±9.16
Elastic cationic niosomes	8.57±3.34	15.41±0.14	23.84±1.88	59.88±1.56
Non-elastic anionic niosomes	2.78±0.81	3.37±0.05	72.90±21.86	82.57±2.02
Elastic anionic niosomes	14.62±0.13	15.32±0.96	37.29±0.67	62.48±5.58
Non-elastic neutral liposomes	3.17±1.96	3.39±0.08	97.24±1.78	90.56±7.24
Elastic neutral liposomes	8.17±0.42	8.72±0.02	35.05±3.88	79.48±9.02
Non-elastic cationic liposomes	2.76±0.76	3.62±0.01	97.71±1.44	91.34±13.62
Elastic cationic liposomes	8.17±0.67	9.69±0.11	41.91±3.94	68.42±5.19
Non-elastic anionic liposomes	2.73±0.61	3.47±0.12	94.63±0.16	79.61±23.15
Elastic anionic liposomes	8.41±1.20	9.42±0.06	41.09±3.93	61.17±10.42

* Cellular uptake (%) values showed in this table were normalized as the uptake efficiency at equal cell number in all samples.

4.1.3. Chemical stability determination of Tat-GFP loaded nanovesicles

GFP stability can be directly related to its fluorescence output, based on the integrity of the fluorophore structure. Its fluorescence intensity can be rapidly quantified in situ using spectrofluorometry (Penna et al., 2004; Mazzola et al., 2006). The % remaining of GFP fluorescence from Tat-GFP loaded in elastic and non-elastic anionic niosomes were shown in Figure 35. The fluorescent intensity of the free Tat-GFP was gradually decreased from 69.42, 45.78 to 33.67% at 1, 2 and 3 months, respectively. When loaded in elastic and non-elastic niosomes, the percentages remaining of Tat-GFP at the 3 month-storage at 30°C were 61.89 and 75.34 % which were higher than the free Tat-GFP of 1.84 and 2.24 times, respectively. According to the entrapment efficiency of Tat-GFP in elastic (32.76%) and non-elastic niosomes (32.09%), it indicated that all of the entrapped Tat-GFP was stable inside the vesicles for over 3 months while the non-entrapped still degraded in the same kinetic as free Tat-GFP. This may be due to the protective effect from the degradation of GFP by loading in nanovesicles (Manosroi et al., 2005). However, the % remaining of Tat-GFP in elastic niosomes at 3 months was less than that in the non-elastic niosomes of 1.22 times. This may be from the prolonged exposure of GFP to ethanol which has been reported to diminish its fluorescence (Zhou et al., 2005). The leakage of Tat-GFP resulting from membrane flexibility of elastic niosomes might be accompanied to the lower stability of Tat-GFP loaded in elastic niosomes comparing to non-elastic niosomes as well.

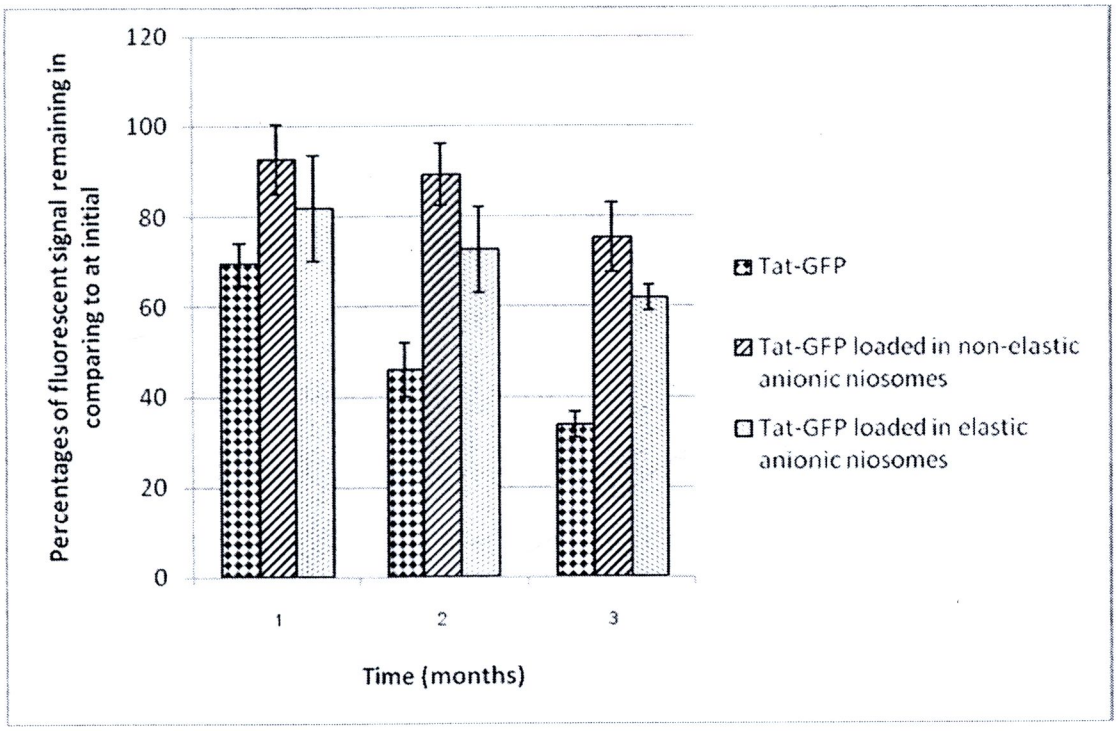

Figure 35 The percentages of fluorescent signal remaining in comparing to at initial of Tat-GFP loaded in elastic and non-elastic anionic niosomes and the non-loaded Tat-GFP when stored at 30±2°C for 3 months.

4.1.4. Development of low toxic elastic anionic niosomes

Based on the cytotoxicity of elastic anionic niosomes containing 25% ethanol, the low toxic elastic anionic niosome was developed by lowering the ethanol content in formulation or using edge activators instead. Sodium cholate (NaC) and sodium deoxycholate (NaDC) were the selected edge activator. After reconstituted in 100 mM phosphate buffer, both elastic and non-elastic empty niosomal dispersion showed best physical stability with no sedimentation for 3 months at room temperature (30±2°C). However, niosomes containing NaDC at 20 and 25 mol% after 3 months gave precipitation. The vesicle sizes and ζ (zeta) potential values of all niosomes were shown in Table 10. Sizes of elastic anionic niosomes were larger than non-elastic niosomes (50.96±10.93 nm) with the size range between 171.94±63.52 nm

to 683.17±331.47 nm. Sizes of elastic anionic niosomes containing ethanol or NaC or NaDC were comparable except the niosomes containing 5% NaDC which showed the largest vesicular size (683.17±331.47 nm). The effect of ethanol concentrations on the vesicular size in this study was conformed to previous study (Verma and Fahr, 2004) which showed that the average vesicular size was increased when the ethanol concentration was increased from 3.3% to 20%. An increase vesicular sizes of niosomes by adding NaC and NaDC was observed. This may be due to the electrostatic repulsion between the negative charges of DP and NaC or NaDC (Persson et al., 2001). The zeta potential values of all elastic anionic niosomes were more negative than the non-elastic anionic niosomes owing to ethanol and NaC or NaDC which may impart the negative charges to the vesicles (Choi and Maibach, 2005; Hiruta et al., 2006). The morphology of non-Tat-GFP loaded and Tat-GFP loaded elastic anionic niosomes (with 1 mol% NaC) were shown in Figure 36. Both Tat-GFP loaded and non-Tat-GFP loaded elastic anionic niosomes were large unilamellar vesicles (LUVs) with spherical shape. The flat-contact was showed at the adhesion surface between vesicles. Fluorescent spots were detected in Tat-GFP loaded elastic anionic niosomes with high proportion of fluorescent at vesicular membrane.

The DI of all formulations was shown in Table 10. They were increased when the ethanol concentrations were increased from 5% to 25%. Ethanol might interact with the polar head-group region of the surfactant molecules in niosomes, resulting in the reduction of melting point, thereby increasing the fluidity of the vesicles (Touitou et al., 2000; Manosroi et al., 2009).

Table 10 Vesicle sizes, zeta potential and deformability index (DI) of blank elastic and non-elastic anionic niosomes (Tween 61/CHL/DP at 1:1:0.05 molar ratio) containing ethanol, NaC or NaDC at various concentrations

Niosomal formulations	Size (nm)	Zeta potential (mV)	DI
Non-elastic anionic niosomes	50.96±10.93	-4.73±0.94	4.81±0.76
Elastic anionic niosomes containing :			
5% v/v ethanol	221.50±6.48	-8.73±0.45	2.01±0.35
10% v/v ethanol	307.20±83.84	-7.79±0.17	5.59±0.67
15% v/v ethanol	339.40±12.46	-17.4±2.51	7.25±0.03
20% v/v ethanol	269.30±39.08	-17.00±3.42	10.53±0.02
25% v/v ethanol	341.20±64.35	-9.08±0.28	10.92±0.13
1 mol% NaC	221.57±84.65	-6.45±2.76	5.68±5.73
2.5 mol% NaC	171.94±63.52	-6.89±4.71	8.09±9.51
5 mol% NaC	336.87±239.32	-8.58±1.44	7.14±9.66
10 mol% NaC	429.90±294.09	-9.49±2.9	5.96±4.23
15 mol% NaC	307.60±18.52	-9.93±2.47	2.79±2.69
20 mol% NaC	212.08±114.5	-12.60±1.54	0.69±0.61
25 mol% NaC	273.40±8.56	-9.32±1.54	1.38±0.81
5 mol% NaDC	683.17±331.47	-10.80±1.89	1.87±2.03
10 mol% NaDC	258.13±78.44	-10.90±1.01	3.71±4.41
15 mol% NaDC	349.90±47.85	-11.10±1.98	0.92±1.28
20 mol% NaDC	258.87±65.32	-11.10±1.6	2.04±2.84
25 mol% NaDC	278.5±18.73	-11.70±1.01	1.08±0.94

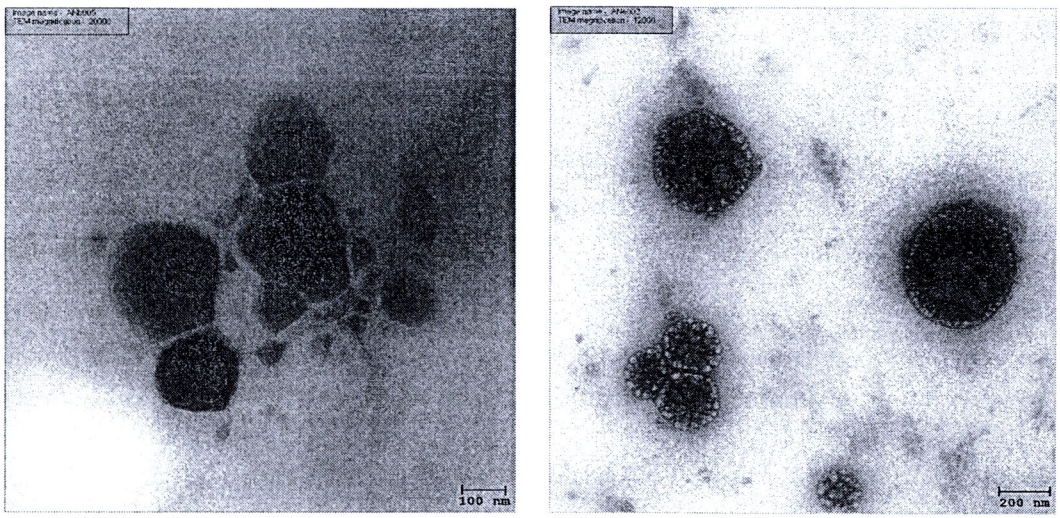

(a) (b)

Figure 36 The negative staining TEM images of (a) blank elastic anionic niosomes (Tween61/CHL/DP/NaC at 1:1:0.02 molar ratio, 1 mol% NaC) (b) Tat-GFP loaded elastic anionic niosomes

Elastic anionic niosomes containing edge activators showed the highest DI values of 8.09±9.51 and 3.71±4.41 for 2.5 mol% NaC and 10 mol% NaDC, respectively which were about 1.68 and 0.77 times of non-elastic anionic niosomes. These edge activators may decrease the transition temperature (T_m) of the vesicles and induce the phase transition of the vesicles to liquid crystalline phase resulting in the increase of vesicle elasticity. However, after the maximum DI value, the deformability decreased when the edge activator concentrations increased. This may be due to the abolishment of the pre-transition endotherm of the vesicles resulting in the increase of vesicular rigidity (Maghraby et al., 2004). Non-elastic anionic niosomes also showed some elastic property because of not only their small vesicle sizes which may be easily with higher amount extruded through the 50 nm polycarbonate membrane, but also the elastic properties from the component of

Tween 61, a surfactant in polysorbate group which can also act as an edge activator (Maghraby et al., 2004).

Entrapment efficiencies of Tat-GFP loaded in vesicles were in the range of 32.09±0.09 to 88.14±5.83% (Table 11). Higher entrapment efficiency (33.34±12.78 to 47.02±15.47%) in ethanol containing niosomes than the non-elastic niosomes (32.09±0.09%) might be due to the solubility enhancement of ethanol on TG that may facilitate the entrapment (López-Pinto et al., 2005). Niosomes containing NaC (32.36±42.72 to 81.81±10.84%) and NaDC (41.07±7.76 to 88.14±5.83%) also showed higher entrapment efficiency than the non-elastic vesicles (32.09±0.09%). This may be due to the larger vesicular size from the incorporation of NaC and NaDC in the niosomal membranes resulting in the higher entrapment amount of Tat-GFP in the hydrophilic core (Brgles et al., 2008).

Table 11 Entrapment efficiencies of Tat-GFP loaded in different elastic vesicular formulations

Niosomal formulations	**Entrapment Efficiency (%)**
Non-elastic anionic niosomes (Tween 61/CHL/DP at 1:1:0.05 molar ratio)	32.09±0.09
Elastic anionic niosomes containing :	
5% v/v ethanol	33.34±12.78
10% v/v ethanol	32.36±5.63
15% v/v ethanol	47.02±15.47
20% v/v ethanol	44.98±9.56
25% v/v ethanol	32.76±5.85
1 mol% NaC	32.36±42.72
2.5 mol% NaC	54.29±10.42
5 mol% NaC	66.83±19.49
10 mol% NaC	62.58±22.08
15 mol% NaC	81.81±10.84
20 mol% NaC	74.51±13.49
25 mol% NaC	68.96±18.99
5 mol% NaDC	78.39±11.92
10 mol% NaDC	41.07±7.76

Table 11 Entrapment efficiencies of Tat-GFP loaded in different elastic vesicular formulations (continued)

Niosomal formulations	Entrapment Efficiency (%)
15 mol% NaDC	82.50±9.43
20 mol% NaDC	84.21±9.18
25 mol% NaDC	88.14±5.83

4.1.5. Cellular uptake and cytotoxicity

The enhancement of cellular uptake of Tat-GFP loaded in developed elastic anionic niosomes in comparing to the non-elastic anionic niosomes in HT-29 and KB cells were demonstrated (Table 12). All elastic vesicles showed similar uptake efficiency of Tat-GFP in the range of 13.28±0.48% to 15.95±0.78% in HT-29 cell and 12.74±1.31% to 16.62±1.53 in KB cells, while the non-elastic anionic niosomes gave only 2.78±0.67 and 3.37±0.12% in HT-29 and KB cells, respectively. The enhancement of cellular internalization of Tat-GFP might be due to the ethanol or edge activators (NaC/NaDC) composition in the elastic niosomal formulation. Ethanol could increase membrane permeability by interact with the hydrophobic core of Tween 61 and cholesterol in the vesicular membrane (Mizoguchi and Hara, 1998), while the edge activators (NaC/NaDC) have the steroidal backbone similar to cholesterol that can not only have an edge activating effect, but also a vesicular membrane stabilizing effect. These edge activators can intercalate into the vesicular membrane resulting in the disordering of the bilayers thereby producing the thinner and flexible vesicles that may facilitate the cellular uptake (Heerklotz, 2008).

The effects of various concentrations of ethanol and edge activators (NaC/NaDC) in elastic niosomes on the viability of HT-29 and KB cells were

investigated by the SRB assay. Viability of both cell lines decreased when the concentrations of ethanol and edge activators increased (Table 12). However, the elastic anionic niosomes containing 1 mol% NaC showed the highest cell viability of 92.32±3.82 and 96.62±5.96% in HT-29 and KB cells, respectively, followed by the ethanol and NaDC containing elastic niosomes. NaC has been reported as the least toxic edge activator in comparing to NaDC and Tween 80. However, the mechanism of higher toxicity of NaDC was still unknown (Lee et al., 2005). For ethanol, its high contents may increase the leakage of cell membrane leading to the decrease of cell viability (Baker and Kramer, 1999).

4.1.6. Transdermal absorption study

Due to the restriction of niosomal formulation for oral administration, transdermal absorption study was performed to evaluate the delivery potential of this developed system. Transdermal absorption of Tat-GFP loaded in elastic anionic niosomes containing 1% NaC which demonstrated high cellular uptake with lowest cytotoxicity was compared with GFP, Tat-GFP fusion protein and Tat-GFP fusion protein loaded in non-elastic anionic niosomes. Cumulative amounts ($\mu g/cm^2$) and fluxes ($\mu g/cm^2h$) of GFP or Tat-GFP from various systems in SC, VED and receiver compartment solution at 6 hrs were shown in Table 13. Both unloaded and loaded Tat-GFP were found in the receiving chamber solution. Tat-GFP loaded in 1 mol% NaC elastic anionic niosomes gave the highest cumulative amounts (62.75 ± 2.68 $\mu g/cm^2$) and fluxes (10.46 ± 3.45 $\mu g/cm^2h$) in the receiving chamber which were about 2 folds higher than Tat-GFP loaded in non-elastic anionic niosomes. This has demonstrated the transdermal enhancement of Tat-GFP when loaded in elastic vesicles composed of 1 mol% NaC. The cumulative amounts and fluxes of Tat-GFP

in buffered solution were similar to Tat-GFP loaded in the non-elastic vesicles, but higher than GFP in buffered solution. This may be due to the presence of the Tat peptide that contained highly positive charged amino acids which can facilitate the endocytosis of Tat-GFP (Fawell et al., 1994; Tseng et al., 2002). Also, NaC in the elastic vesicles can influence the lipid bilayer fluidity of SC and improve the partitioning of Tat-GFP across the SC into the deeper layers of the skin without the accumulation in VED (Jain et al., 2005).

Table 12 Cellular uptake and cytotoxicity of Tat-GFP loaded in elastic and non-elastic niosomes in HT-29 and KB cells

Niosomal formulations	**% uptake***		**%viability**	
	HT-29	**KB**	**HT-29**	**KB**
Non-elastic anionic niosomes (Tween 61/CHL/DP at 1:1:0.05 molar ratio)	2.78±0.67	3.37±0.12	72.90±21.86	82.57±2.02
Elastic anionic niosomes containing :				
5% v/v ethanol	14.56±0.99	15.55±0.65	76.44±6.09	84.33±10.52
10% v/v ethanol	13.78±0.44	15.76±1.04	65.69±2.64	82.46±10.88
15% v/v ethanol	14.31±0.26	15.43±1.23	52.55±17.73	79.89±2.25
20% v/v ethanol	14.76±0.51	16.16±1.11	45.04±5.02	70.55±3.35
25% v/v ethanol	14.62±0.07	15.32±0.96	37.29±0.67	62.48±5.58
1 mol% NaC	14.99±0.31	16.54±0.52	92.32±3.82	96.62±5.96
2.5 mol% NaC	14.34±0.18	16.42±0.58	90.7±4.66	89.59±3.11
5 mol% NaC	14.15±0.29	16.62±1.53	85.44±5.41	87.15±14.46
10 mol% NaC	14.94±0.49	16.47±0.94	76.49±10.04	82.57±7.83
15 mol% NaC	15.14±0.49	13.49±1.08	34.41±26.76	68.87±10.50
20 mol% NaC	13.76±0.38	14.98±0.84	29.81±1.77	54.62±7.87
25 mol% NaC	13.66±0.75	14.31±0.64	23.51±7.48	57.14±5.11
5 mol% NaDC	14.85±0.12	12.74±1.31	26.98±3.55	36.14±5.91
10 mol% NaDC	13.28±0.48	15.89±1.49	15.82±13.65	39.04±13.49
15 mol% NaDC	13.46±0.57	16.21±0.30	10.77±9.69	28.99±9.67
20 mol% NaDC	15.95±0.78	14.21±0.29	29.35±10.95	40.06±8.78
25 mol% NaDC	14.91±0.27	15.45±1.31	26.98±12.21	45.07±10.10

* Cellular uptake (%) values showed in this table were normalized as the uptake efficiency at equal cell number in all samples.

Table 13 The cumulative amounts ($\mu g/cm^2$) and fluxes ($\mu g/cm^2 h$) of GFP and Tat-GFP from various systems in SC, VED and receiver compartment following transdermal absorption across excised rat skin at 6 hours by vertical Franz diffusion cells

Systems	Cumulative amounts ($\mu g/cm^2$) ± SD			Fluxes ($\mu g/cm^2 \cdot h$) ± SD		
	SC	VED	Receiver compartment	SC	VED	Receiver compartment
GFP solution in 100 mM phosphate buffer (pH 7.0)	24.15 ± 7.28	17.92 ± 0.78	22.61 ± 2.87	4.02 ± 1.21	2.99 ± 0.26	3.77 ± 0.48
Tat-GFP solution in 100 mM phosphate buffer (pH 7.0)	4.86 ± 0.55	6.06 ± 0.70	28.50 ± 12.07	0.81 ± 0.09	1.01 ± 0.70	4.75 ± 1.47
Tat-GFP loaded in non-elastic anionic niosomes (Tween 61/CHL/DP at 1:1:0.05 molar ratio)	22.03± 4.01	0	30.24 ± 4.81	3.67 ± 2.33	0	5.04 ± 0.80
Tat-GFP loaded in elastic anionic niosomes (Tween 61/CHL/DP at 1:1:0.05 molar ratio) containing 1 mol% of NaC	8.59 ± 1.33	0	62.75 ± 2.68	1.43 ± 0.22	0	10.46 ± 3.45

4.2. Tat/GFP, VP/GFP and VP/Tat/GFP mixture

4.2.1. Evaluation of simple mixing method as cargoes transport strategy

In Figure 37, when the incubation time was increase from 1 to 5 hour, both Tat/GFP and Tat-GFP did not showed significant difference in uptake efficiency which demonstrated the rapid uptake enhancement of GFP by Tat into HT-29 cells and reach the maximum within 1 hour. The rapid internalization of Tat (< 4 min) in fibroblast cells (Ziegler et al., 2005) and the uptake of streptavidin by Tat within 5 min have been reported (Rinne et al., 2007).

Cellular uptake of Tat-GFP and Tat/GFP into HT-29 cells after 1 hr incubation was 5.21±0.24% and 9.31±0.05% which was 2.38 and 4.25 folds of GFP, respectively. Several studies revealed the capability of CPP such as Pep-1 and polyarginine to deliver different peptides, proteins, and antibodies into different cells, *in vivo* and *in vitro,* without any chemical coupling between the cargo and CPP (Morris et al., 1999; Gros et al., 2006; Hu et al., 2009), which were similar to this study using Tat as a CPP. Higher uptake efficiency of Tat/GFP mixture than the fusion protein might be due to the higher flexibility and mobility of CPP-cargo delivery by physical mixing strategy in Tat/GFP than the covalent linkage in Tat-GFP which cause the rigid construction and might be difficult for Tat moiety to expose to cell membrane (Liu et al., 1999; Myrberg et al., 2007). The smaller hydrodynamic particle sizes of Tat/GFP (421.5±83.79 nm) than Tat-GFP (515.0±45.68 nm) determined by DLS equipment might also facilitate cellular internalization (Nabeshi et al., 2010).

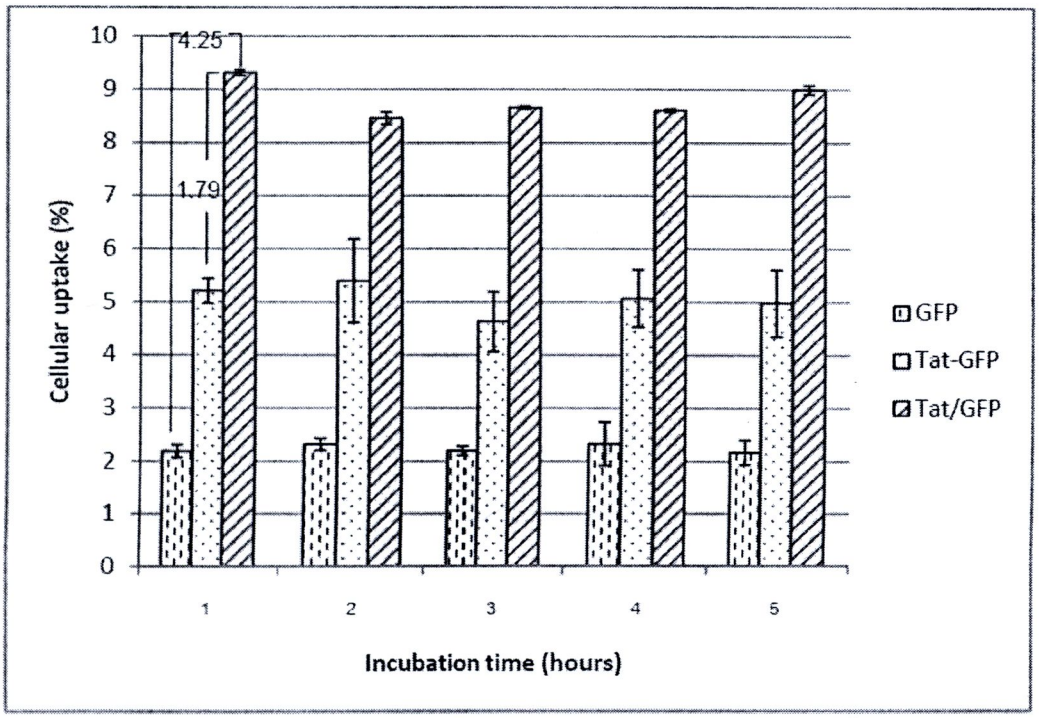

Figure 37 Comparison of cellular uptake at various time intervals of GFP, Tat:GFP fusion protein (Tat-GFP) and mixture (Tat/GFP) into HT-29 cells. The concentration of GFP and Tat both in fusion and mixture form at 1:1 molar ratio were 1 μM. The folds of Tat/GFP uptake in comparing to Tat-GFP and GFP at 1 hour were labeled above the bar chart.

The results of the permeation study in HT-29 cells were shown in Figure 38. Since the amount of permeated GFP at 1 μM was out of detection limit, the concentration at 2 μM was used in transepithelial study. The percentage of fluorescent protein which permeated across HT-29 cells demonstrated the time-dependent permeation pattern in all samples. Tat-GFP showed the highest permeation across HT-29 cells at all incubation time. The percentage of Tat-GFP permeated through the Transwell™ plate after 5 hr incubation was 30.19% which was 1.3 and 1.2 fold of the permeated GFP and Tat/GFP, respectively. This might be due to the

increase in stability of the fusion protein which contain poly-histidine residue as tag for purification and the covalent bonding of Tat-GFP, a recombinant protein which is stronger than the weak bonding such as ionic bonding and Van der Waals forces. The replacing of amino acid Arg, Lys, Leu, Phe, Tyr, and Trp at the N-terminal with others has been reported to increase the protein half-life. The ability of fusion protein to sequester away from cytosolic proteolytic degradation machinery has also reported (Lin-Lee et al., 2002). In Tat/GFP, the mixture might remain in endosomal compartment resulting in the highest intracellular fluorescent signal in the uptake study (Figure 37).

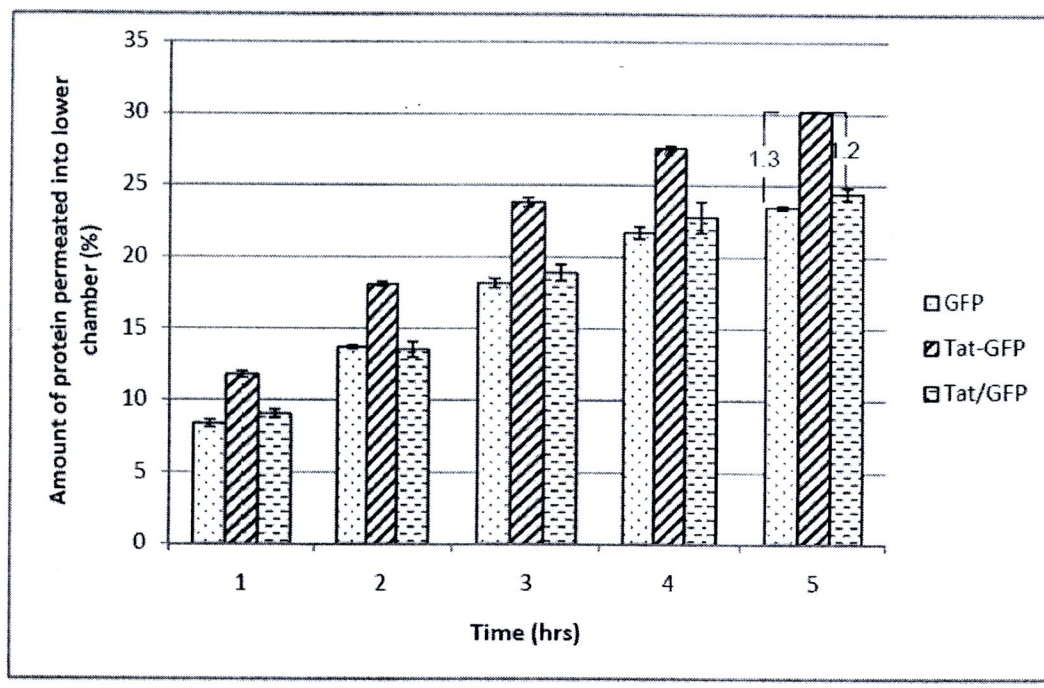

Figure 38 Transepithelial permeation of GFP, Tat-GFP and Tat/GFP through HT-29 cells cultured in Transwell™ plate. Percentages of protein in lower chamber comparing with the total protein added into each well were presented. The concentration of all samples was equivalent to 2 μM of GFP. Tat/GFP at 1:1 molar ratio was used.

Cumulative amounts ($\mu g/cm^2$) and fluxes ($\mu g/cm^2h$) of GFP, Tat-GFP and Tat/GFP in SC, VED and receiving chamber at 6 hrs were shown in Table 14. All samples could permeate through the rat skin and found in the receiving compartment. Tat/GFP demonstrated the highest cumulative amounts (0.204±0.021 $\mu g/cm^2$) and fluxes (0.034±0.004 $\mu g/cm^2h$) in the receiving chamber which were about 5.57 and 8.87 folds of Tat-GFP fusion protein and GFP, respectively. This might be due to the higher positive charge (zeta potential = -9.62±1.09 mV) on the molecular surface of Tat/GFP than the Tat-GFP (zeta potential = -11.6±2.44 mV); zeta potential value of MQ water was -17.60±7.46 mV. The importance of positive surface charges for the effective transdermal delivery for the electrostatic interaction with the skin barrier has been reported (Kim et al., 2010). The amount of GFP and Tat-GFP fusion protein were not detected in VED. At 6 hr, the amount of GFP in Tat/GFP detected in receiving chamber was 10.04% of the applied amount which was 5.57 folds of Tat-GFP. The smaller particle sizes of Tat/GFP might also facilitate the transdermal absorption, since the reduction in particle sizes and the increase of SC permeation across mouse skin has been reported (Nabeshi et al., 2010). As known, the amount of sample detected in receiving chamber represented the possibility of sample to cross the skin barrier to circulation after transdermal application (Amsden and Goosen, 2004). Then, the physical mixing of Tat with targeted peptide might be applicable for the development of transdermal delivery system.

Table 14 Transdermal absorption across excised rat skin of GFP, Tat-GFP fusion protein and Tat/GFP mixture at 6 hours in stratum corneum (SC), viable epidermis and dermis (VED) and receiver compartment of vertical Franz diffusion cells

Systems	Cumulative amounts (μg/cm^2) ± SD (Percentage of initial [%])			Flux (μg/cm^2 ·h) ± SD		
	SC	VED	Receiver compartment	SC	VED	Receiver compartment
GFP	0.024 ± 0.007 (1.18%)	0 (0%)	0.023 ± 0.003 (1.13%)	0.004 ± 0.001	0	0.0038 ± 0.000
Tat-GFP fusion protein	0.005 ± 0.000 (0.25%)	0 (0%)	0.036 ± 0.012 (1.77%)	0.0008 ± 0.0000	0	0.006 ± 0.001
Tat/GFP mixture	0.178 ± 0.010 (8.76%)	0.194 ± 0.024 (9.54%)	0.204 ± 0.021 (10.04%)	0.029 ± 0.002	0.032 ± 0.004	0.034 ± 0.004

Note: Each value represented the mean ± S.D. (n = 3)

4.2.2. Cellular uptake study of Tat/GFP, VP/GFP and VP/Tat/GFP mixture

Enhancement of GFP translocation by co-incubation with VP or Tat peptide at various molar ratios was demonstrated. Both VP and Tat dramatically enhanced the cellular uptake efficiency of GFP into HT-29 and KB cells (Figure 39). By mixing with VP, GFP cellular uptake into HT-29 and KB cells were in the range of 8.52-8.73% and 8.58-8.92% which were 3.89-3.98 folds and 3.90-4.05 folds of GFP, respectively. When mixing with Tat, the uptake efficiency of GFP into HT-29 and KB cells were in the range of 9.29-10.05% and 9.67-11.19% which were 4.24-4.59 folds and 4.39-5.09 folds of GFP, respectively. No significant difference in cellular uptake efficiency of GFP when VP or Tat was mixed with GFP at different molar ratio of 6:1 to 1/3:1. It was known that Tat peptide can efficiently delivered non-covalently conjugated protein, RNA and DNA into living cells or tissues in fully active forms (Wang et al., 2006; Chen et al., 2007). The interaction between CPPs and cargo protein in non-covalently protein transduction has been reported (Hu et al., 2009). An enhancement of GFP cellular uptake by Tat comparing with VP peptide might be due to the higher number of positively charged amino acids of Tat which is needed to facilitate the delivery of large proteins (Furuhata et al., 2006). The hydrophobic property of VP which is required for cellular internalization (Watkins et al., 2009) and the ability of VP1 BC loop sequence to bind with PVR on gastrointestinal epithelial cells might responsible for the GFP uptake enhancement by VP. Moreover, the co-incubation of GFP with both VP and Tat peptide gave similar uptake efficiency as with either VP or Tat alone indicated no synergistic effect of VP and Tat on GFP translocation into HT-29 and KB cells. Although HT-29 cells

expressed higher amount of PVR than KB cells (Figure 40), similar GFP cellular uptake efficiency into HT-29 and KB cells by VP were observed. This might be due to the higher negative charge on cell surface of HT-29 cells than the KB cells which resulting in repulsion force between negative charge on cell surface and VP/GFP mixture.

Part 5 : *In vitro* calcitonin activity of Tat/sCT, VP/sCT and VP/Tat/sCT mixtures

5.1. Physical properties of the mixture

5.1.1. Sizes and zeta potential determination

Particle sizes and zeta potential values of sCT, Tat, VP and Tat/VP/sCT mixtures at various molar ratios were shown in Table 15. Particle size of sCT, Tat and VP at the same molar concentration were 235.90±77.36, 1,106.00±191.90 and 502.60±104.10 nm, respectively. All mixtures showed smaller particle size than the size of their parent peptides in the system indicating the dense and homogeneous arrangement between peptide molecules in the mixture (Lee et al., 2010). The increase in zeta potential value of sCT (-5.92±1.36) and Tat (-3.03±2.53) comparing with MQ water (-17.6±7.46 mV) indicating their charge positivity, while VP showed negative charge due to the slightly higher negativity zeta potential value (-17.80±2.73) than MQ water. Tat/sCT mixtures at all molar ratios gave positive zeta potential values (11.4±0.79 to 13.9±0.32 mV) from the totally charge between Tat and sCT with higher positive charge in the higher Tat proportion, whereas the VP/sCT and VP/Tat/sCT mixtures demonstrated negative zeta potential value from the charge negativity of VP molecule.

A.

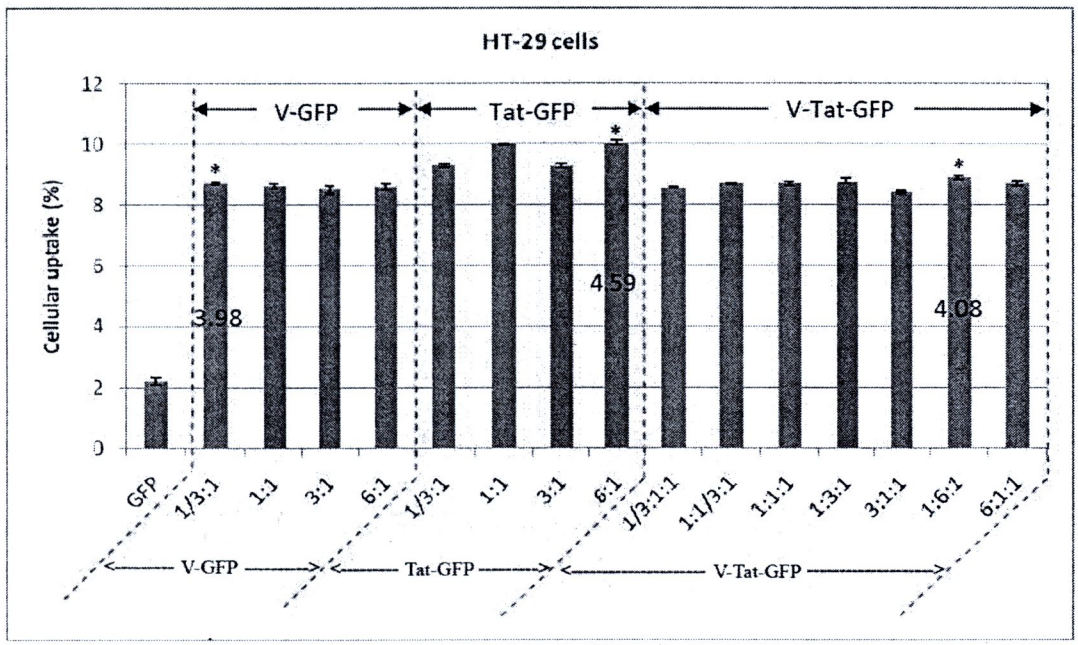

B.

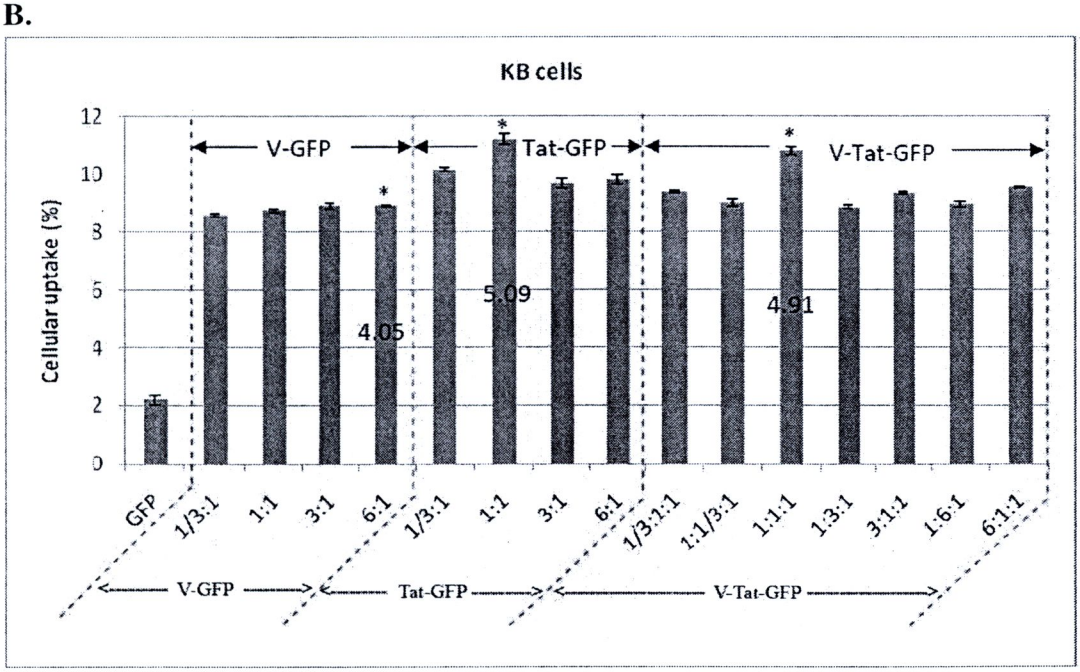

Figure 39 Cellular uptake (%) of GFP, mixture of GFP, VP1 BC loop (VP) and Tat into HT-29 (A) and KB cells (B). The concentration of GFP was 1 μM at all molar ratio. The molar ratio with the highest GFP uptake in each mixture was specified by asterisk and folds of uptake comparing with GFP alone were labeled in the center of the bar.

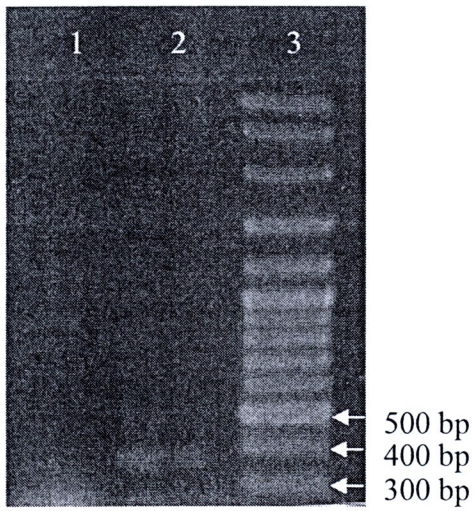

Figure 40 Agarose gel electrophoresis of poliovirus receptor (PVR, CD155; 349 bp) transcripts amplified by RT-PCR from KB cells (lane 1) and HT-29 cells (lane 2). Lane 3 was the 100 kb DNA ladder.

5.1.2. Differential scanning calorimetry (DSC) and Fourier transform infrared spectroscopy (FT-IR)

The physico-chemical characteristics of Tat/sCT, VP/sCT and VP/Tat/sCT mixtures were determined by DSC and FT-IR spectroscopy. Figure 41 showed the DSC thermograms of sCT, Tat, VP and the mixtures of Tat/sCT, VP/sCT and VP/Tat/sCT mixture. sCT showed a single exothermic peak at 155.84°C, whereas Tat demonstrated some alterations at over 200°C. In addition, VP gave a single exothermic peak at 166.98°C. Tat/sCT, VP/sCT and VP/Tat/sCT mixtures showed no exothermic peak at the temperature understudied. The disappearance of sharp exothermic peak of single peptide in the mixtures indicated the physico-chemical interaction among sCT, VP and Tat (Brown et al., 1999; Kumar et al., 2008). Figure 42 showed the FT-IR spectra of sCT, Tat, VP and mixtures of Tat/sCT, VP/sCT and VP/Tat/sCT. In Figure 42A, sCT showed one sharp peak of the

stretching vibration of hydroxyl group (–OH) at 3307.99 cm^{-1} and 2 peaks of N-H bending at 1657.95 and 1538.25 cm^{-1}, respectively. Two strong peaks at 2350.38 and 661.89 cm^{-1} observed in sCT sample were from asymmetrical stretching and symmetrical bending of C=O, respectively. C-N stretching peak of amide was detected at 1415.53 cm^{-1}, while the vibration peaks of C-O from phenol group of tyrosine were recorded at 1254.20 and 1118.94 cm^{-1}. In Tat, besides the O-H stretching, N-H bending and C-N stretching peak of amide as found in sCT, C-N stretching peak of amine and C-H rocking peaks were also detected at 1195.58 cm^{-1} and 599.96-805.19 cm^{-1}, respectively (Figure 42B). For VP, both C-N stretching peak of amide and amine were detected at 1440.41 cm^{-1} and 1193.12 cm^{-1}, respectively. The peaks of N-H bending and O-H stretching were also observed (Figure 42C). Moreover, C-H stretching peak was observed at 2966.20 cm^{-1}. In Figure 42D, the increase in peak intensity at 1100-1200 cm^{-1} and the decrease of C=O stretching peak at 2349.42 cm^{-1} of sCT were observed in Tat/sCT mixture. A slightly decrease of C-N stretching peak and the disappearance of C-H bending of Tat at 1438.16 and 719.73 cm^{-1}, respectively were also detected in Tat/sCT mixture. For VP/sCT and VP/Tat/sCT mixtures, sharp peak of C=O stretching at 2350.38 cm^{-1} of sCT was disappeared and the FT-IR spectrum showed the similar pattern with VP peptide (Fig. 2E and F). This might be resulting from the cage formation around Tat and sCT of hydrophobic residues in VP peptide (Bais et al., 2008). These results indicated some interactions with complex formation among sCT and Tat or VP (Yang et al., 2007b; Lee et al., 2010).

Table 15 Particle sizes (nm) and zeta potential (mV) of sCT, Tat, VP and Tat/VP/sCT mixtures at various molar ratios

Samples	Particle size (nm)	Zeta potential (mV)
Water	-	-17.60±7.46
sCT 100 pg/ml (29.15 pM)	235.90±77.36	-5.92±1.36
Tat 61.22 pg/ml (29.15 pM)	1,106.00±191.90	-3.03±2.53
VP 61.22 pg/ml (29.15 pM)	502.60±104.10	-17.80±2.73
Tat:sCT = 1/3:1	347.80±38.07	11.4±0.79
Tat:sCT = 1:1	222.90±71.28	12.4±6.40
Tat:sCT = 3:1	290.80±54.22	13.0±2.06
Tat:sCT = 6:1	337.00±92.34	13.9±0.32
VP:sCT = 1/3:1	338.80±66.06	-2.53±1.02
VP:sCT = 1:1	340.00±40.3	-7.72±3.10
VP:sCT = 3:1	326.90±23.70	-6.24±1.63
VP:sCT = 6:1	301.20±29.90	-7.54±2.00
VP: Tat:sCT = 1/3:1:1	335.80±30.22	-8.09±3.36
VP: Tat:sCT = 1:1/3:1	380.10±67.95	-12.2±3.33
VP: Tat:sCT = 1:1:1	330.90±68.06	-6.4±5.39
VP: Tat:sCT = 1:3:1	504.90±24.53	-6.2±1.17
VP: Tat:sCT = 1:6:1	398.70±17.46	-2.43±0.28
VP: Tat:sCT = 3:1:1	226.80±4.27	-12.6±4.21
VP: Tat:sCT = 6:1:1	274.20±130.20	-13.9±0.32

Note: In mixture form, the concentration of sCT was fixed at 100 pg/ml

THE NATIONAL RESEARCH COUNCIL OF THAILAND RESEARCH LIBRARY

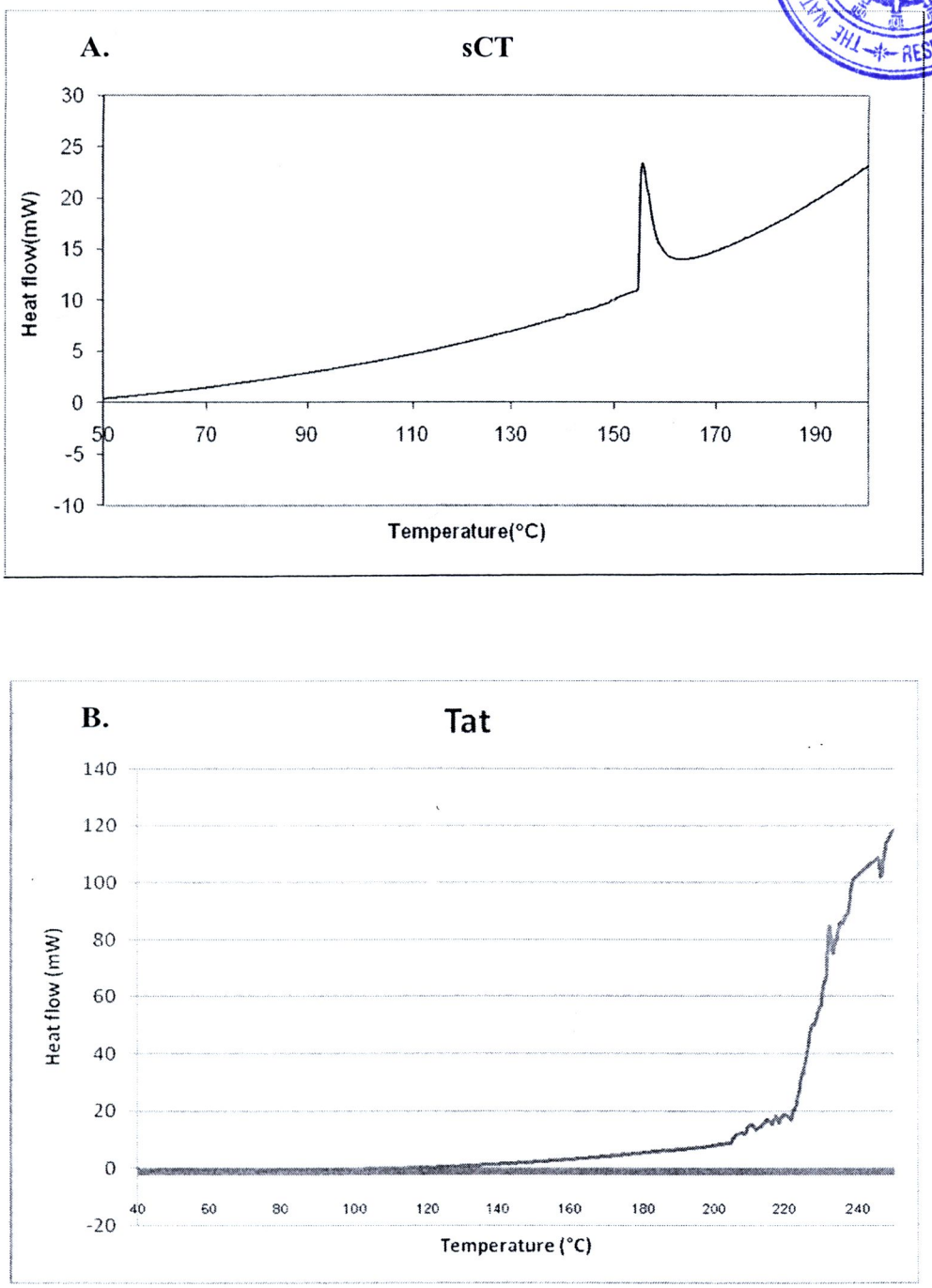

Figure 41 Differential scanning calorimetry (DSC) thermograms of sCT (A), Tat (B) VP (C), Tat/sCT mixture (D), VP/sCT mixture (E) and VP/Tat/sCT mixture (F)

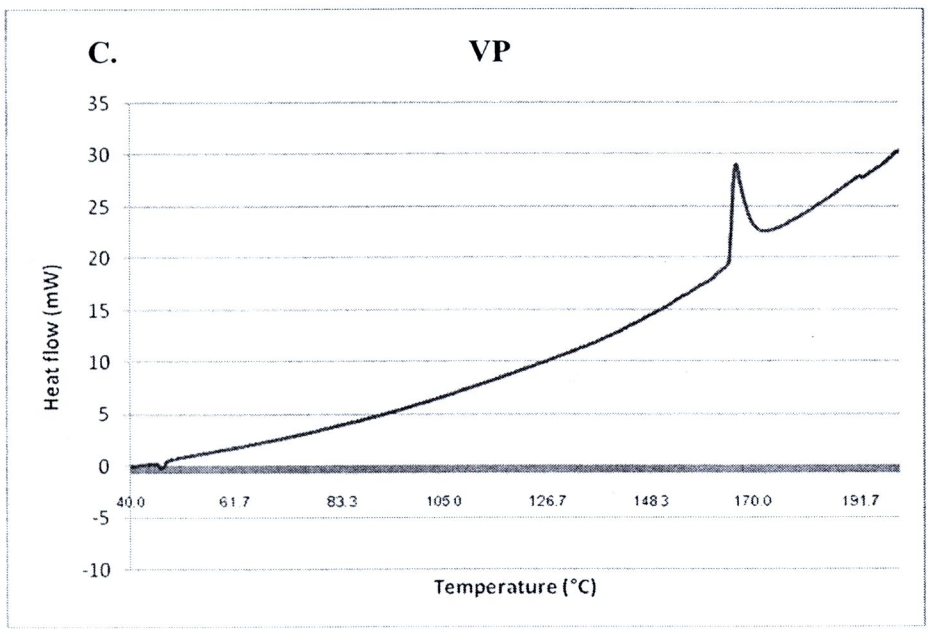

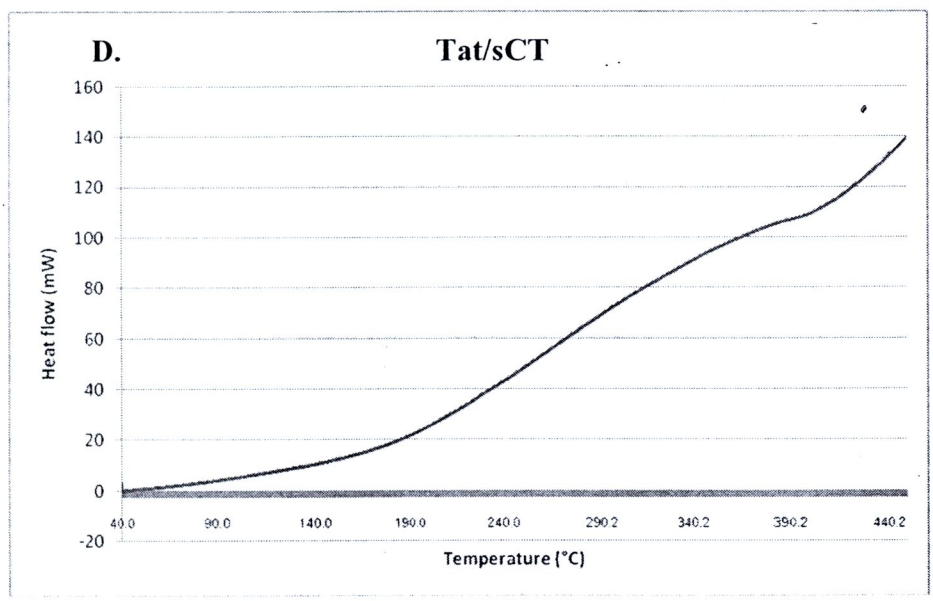

Figure 41 Differential scanning calorimetry (DSC) thermograms of sCT (A), Tat (B) VP (C), Tat/sCT mixture (D), VP/sCT mixture (E) and VP/Tat/sCT mixture (F) (continued)

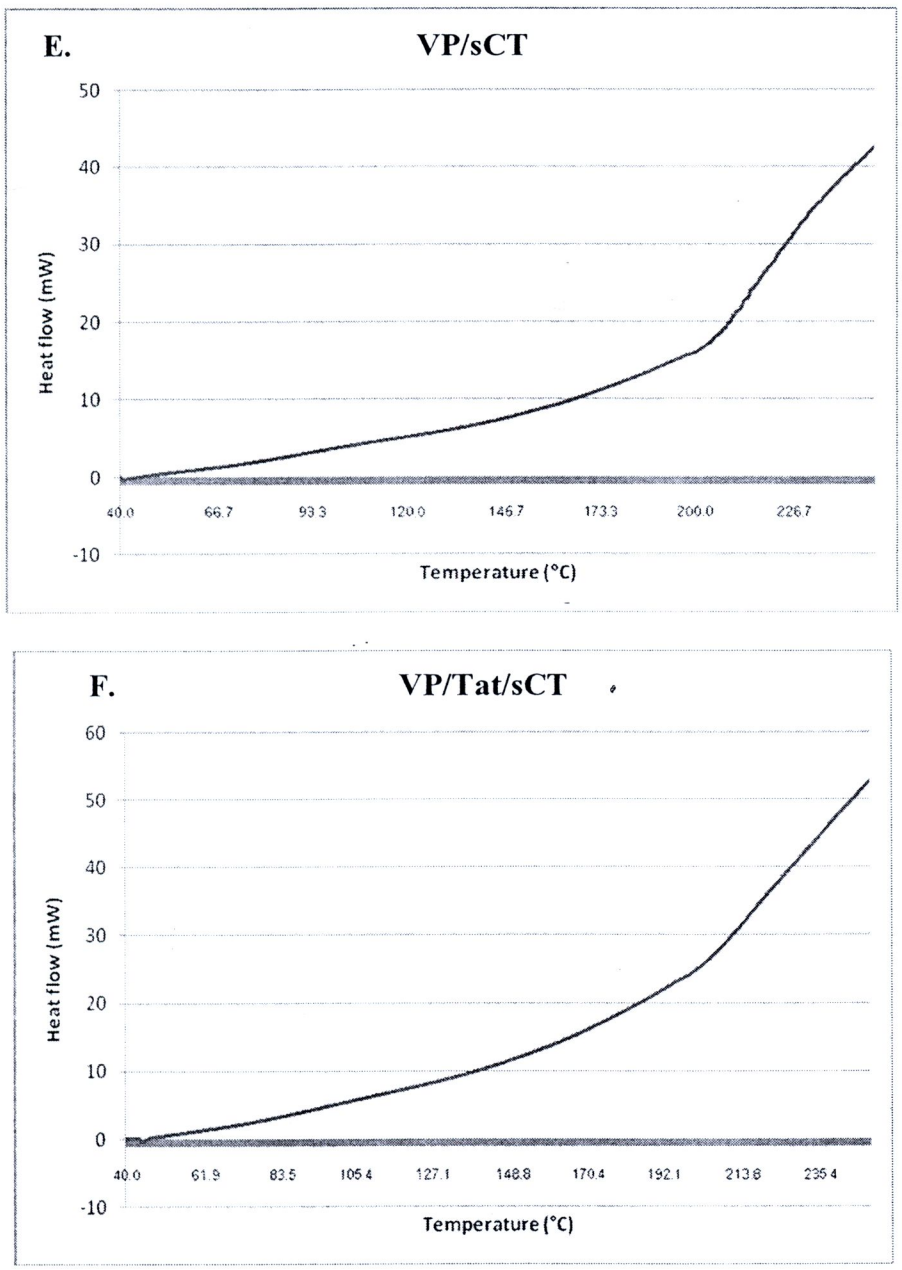

Figure 41 Differential scanning calorimetry (DSC) thermograms of sCT (A), Tat (B) VP (C), Tat/sCT mixture (D), VP/sCT mixture (E) and VP/Tat/sCT mixture (F) (continued)

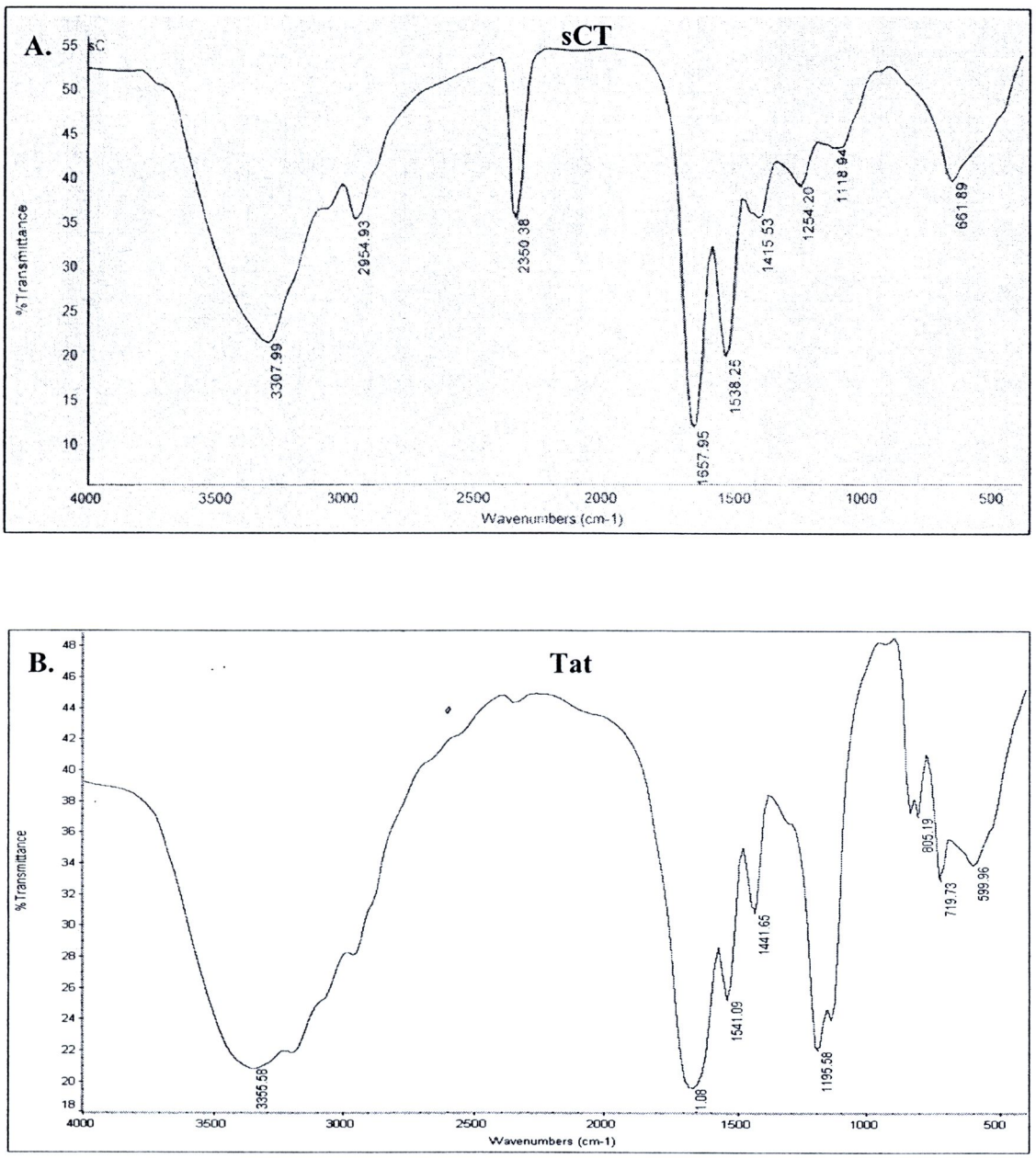

Figure 42 FT-IR spectra of sCT (A), Tat (B) VP (C), Tat/sCT mixture (D), VP/sCT mixture (E) and VP/Tat/sCT mixture (F)

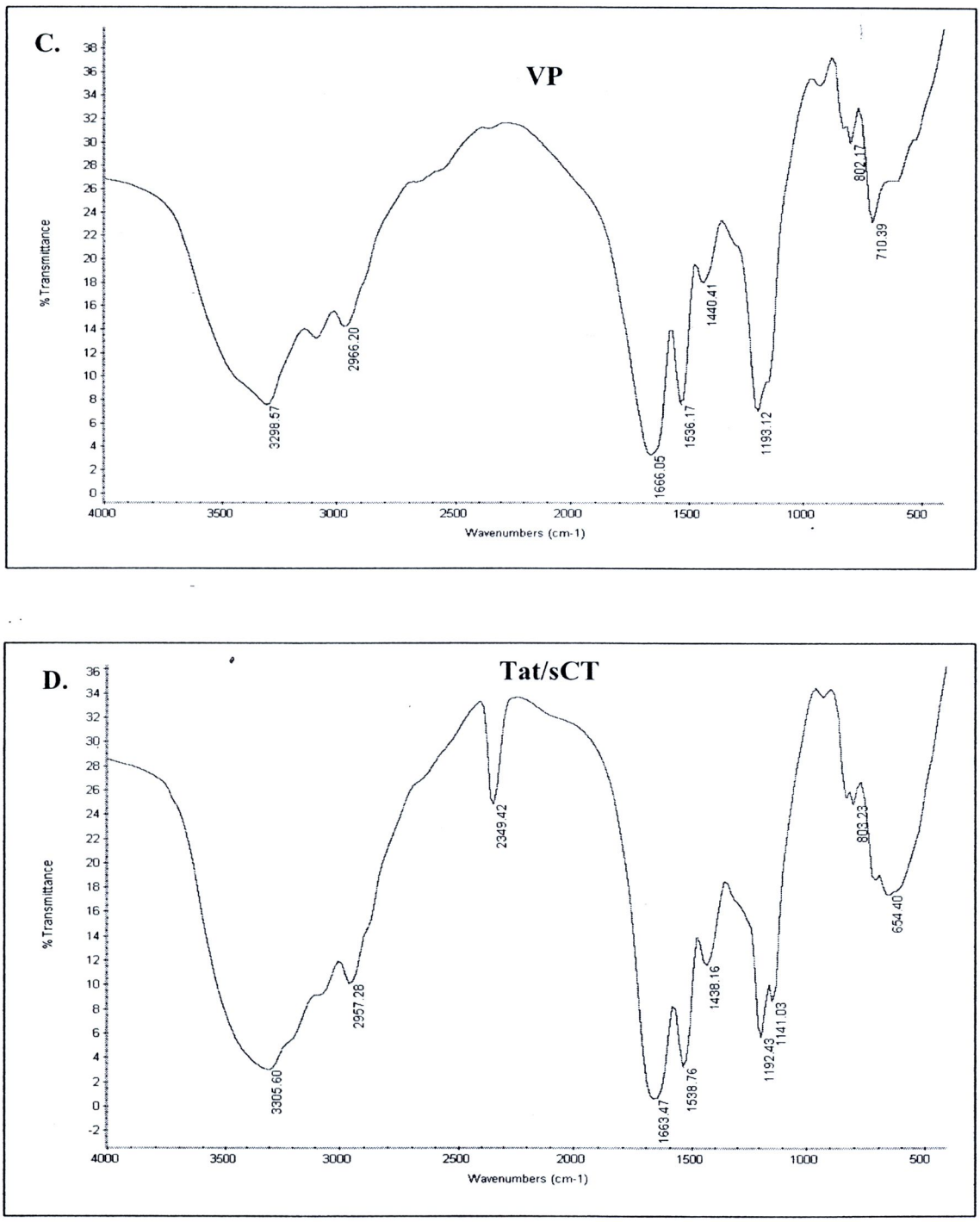

Figure 42 FT-IR spectra of sCT (A), Tat (B) VP (C), Tat/sCT mixture (D), VP/sCT mixture (E) and VP/Tat/sCT mixture (F) (continued)

THE NATIONAL RESEARCH COUNCIL OF THAILAND
RESEARCH LIBRARY

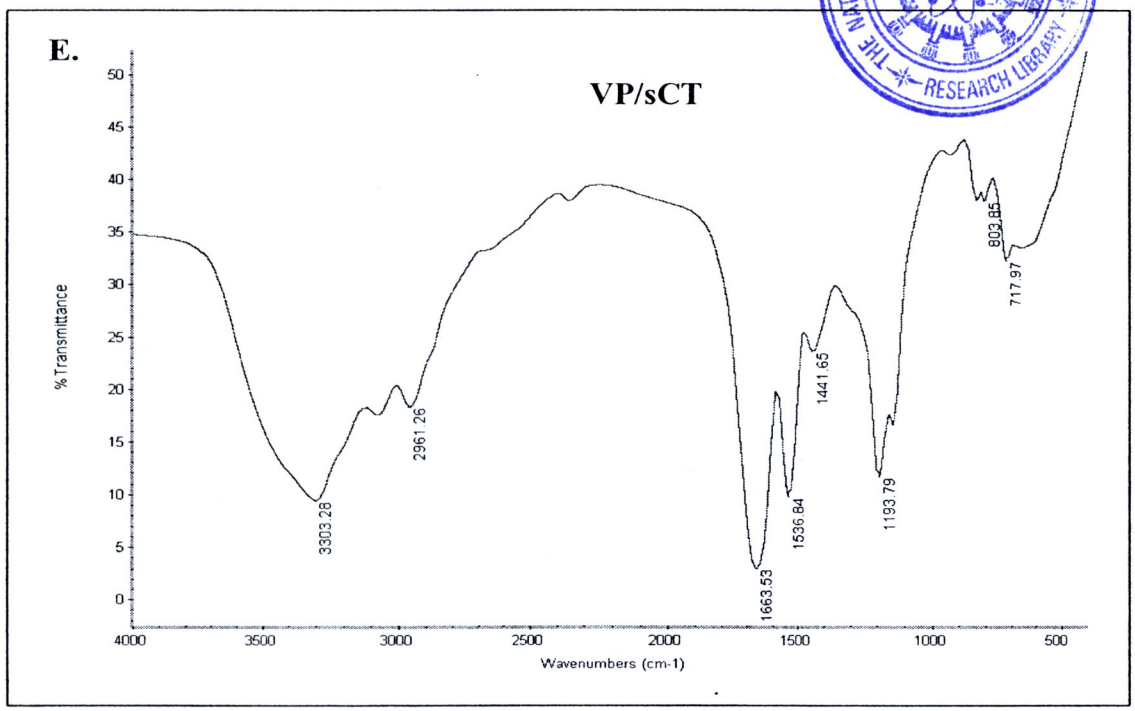

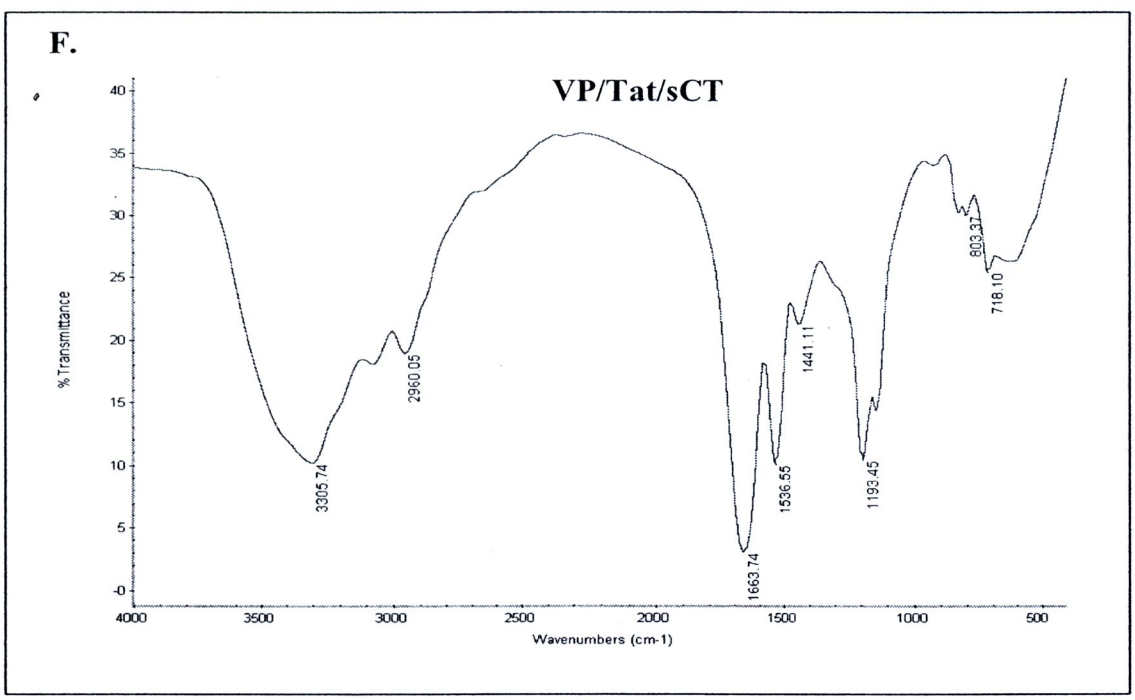

Figure 42 FT-IR spectra of sCT (A), Tat (B) VP (C), Tat/sCT mixture (D), VP/sCT mixture (E) and VP/Tat/sCT mixture (F) (continued)

5.2. *In vitro* calcitonin activity experiment

Most of intracellular calcium is sequestered in mitochondria and endoplasmic reticulum with fluctuate concentration roughly from 100 nM to greater than 1 μM, due to the release from cellular stores or influx from extracellular fluid controlled by parathyroid hormone (PTH) and CT. The extent of intracellular calcium accumulation indicating the extent of CT activity in cellular level is directly related to the concentration of calcium in medium (Harell et al., 1975). In this study, the *in vitro* sCT activity was determined from the increase in intracellular calcium concentration after incubation with samples in medium containing calcium as chloride salt at 0.2 mg/ml. The relative intracellular calcium (%) in HT-29 and KB cells after incubation with samples at various molar ratios were presented in Figure 43. Without Tat or VP, sCT activity could not detect owing to the lack of CTR on the membrane of these cells (Frucht et al., 1992). CTR is a member of a new family of related G-protein coupled receptors which includes the PTH, secretin, and glucagon receptors (Goltzman and Mitchell, 1985; Segre and Goldring, 1993). It is concentrated in the bone, hypothalamus, and kidney. CT activity in non-osteoclast cell transfected with cDNA encoding CTR has been reported (Stroop and Moore, 1995). This indicated the significance of CTR for sCT activity. Hence, some carrier was needed for the translocation of sCT. When mixed with Tat, the activity of sCT was increased in both cell lines with the maximum relative intracellular calcium of 116.46±0.57 and 172.14±4.12% from Tat/sCT mixture at 3:1 and 1:1 molar ratio in HT-29 and KB cell lines, respectively. The increase of sCT activity might be due to the enhancement of sCT uptake and absorption from positive charge of the complex resulting from Tat which could facilitate the electrostatic interaction with cellular surface (Yang et al.,

2007a). The intracellular calcium was remarkably increased by Tat/sCT mixture in KB cells in comparing with HT-29 cells. This can be described by the variation of cytoplasmic and nucleic distribution of Tat in different cell lines (Mueller et al., 2008). VP/sCT mixture at 6:1 molar ratio showed significant increasing of intracellular calcium in HT-29 cells of 152.07% of control. However, VP/sCT mixture could not increase intracellular calcium in KB cells. Since the results of semi-quantitative PVR (CD155) expression of both cells demonstrated the expression of extracellular domain of CD155 (349 bp) was observed in HT-29, but not in KB cells (Figure 40). These could confirm the ligand-receptor mediated cellular delivery of sCT by the interaction between VP and PVR. VP/Tat/sCT mixtures gave the same pattern of sCT activity as either Tat/sCT or VP/sCT mixtures on both cell lines. VP/Tat/sCT mixtures at 6:1:1 molar ratio (the same VP:sCT proportion as VP/sCT mixture 6:1 which gave the highest sCT activity in HT-29 cells) demonstrated the highest intracellular calcium level in HT-29 cells. Also, the VP/Tat/sCT mixtures with Tat/sCT ratio at 1:1 also showed the better sCT activity in KB cells.

Part 6 : *In vivo* calcitonin activity of Tat/sCT, VP/sCT and VP/Tat/sCT mixtures

6.1. Subcutaneous administration of sCT

The hypocalcemic activity of subcutaneously administered sCT as positive control at various doses was evaluated in the rat model. Significant lowering of serum calcium was observed in all doses after 1-2 hr of injection and remained for over 12 hr (Figure 44A). The result was similar to the previously reported about the decreasing of serum calcium within 2 hr after parenteral sCT administration and persists for about 6-8 hr (Azria, 1989).

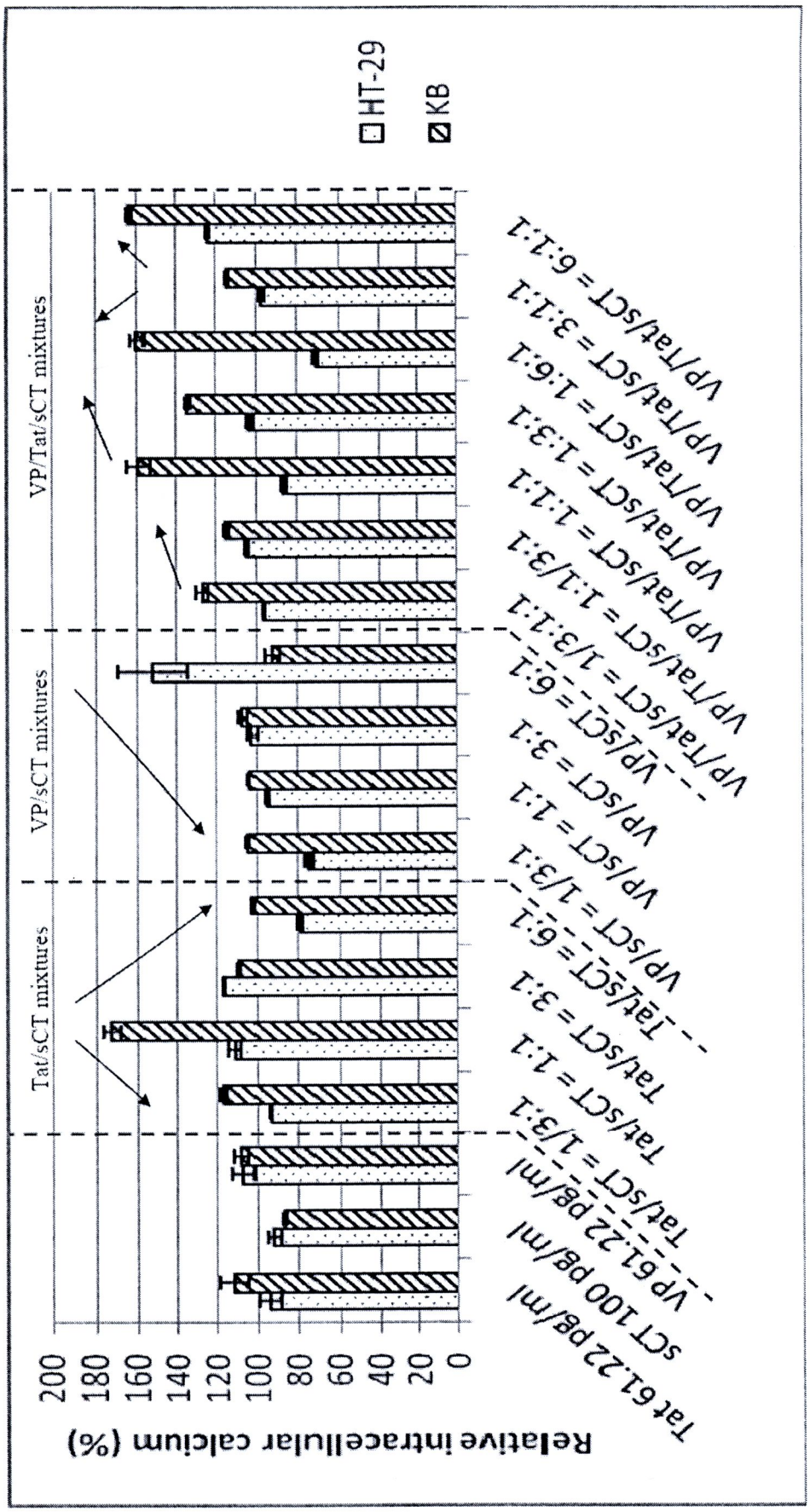

Figure 43 Relative intracellular calcium (%) after incubation with sCT (fixed concentration 100 pg/ml), Tat (61.22 pg/ml), VP (61.22 pg/ml) and Tat/VP/sCT mixtures at various molar ratios. The direction of particle size increasing was indicated by arrow.

The dose at 50 μg/kg was selected for oral administration experiment due to the lowest fluctuation in serum calcium level.

6.2. Oral administration of Tat/sCT, VP/sCT and VP/Tat/sCT mixture

The hypocalcemic activity of oral sCT and mixtures which showed the highest sCT activity in HT-29 and KB cells which were Tat/sCT mixtures at 3:1 and 1:1; VP/sCT mixtures at 6:1 and 3:1; and VP/Tat/sCT mixture at 6:1:1 molar ratio were investigated in rats. Orally administration of sCT at 50 μg/kg showed the decrease in serum calcium with the minimum relative serum calcium of 64.13±2.93% at 1 hr (Figure 44B). Interestingly, Tat/sCT mixture at 1:1 molar ratio demonstrated hypocalcemic effect with the prolonged activity of over 24 hr with the reduction in the serum calcium level of about 18-31% of the control at the dose of 50 μg/kg which was equivalent to 300 IU/kg (6,000 IU = 1 mg; European Pharmacopoeia, 2007). This might be from the slow release of sCT from sCT/Tat complex (Lee et al., 2010). Generally, the therapeutic dose of sCT is in the range of 50-400 IU/day depending on the indication and the greater decrease in serum calcium tends to be found in patient with higher serum calcium level. Serum calcium level after subcutaneous injection of CT generally decreased about 20-30% (Wimalawansa, 1997). The results from this study indicated that these mixtures could be considered as a substituted oral dosage form for sCT administration. Moreover, oral Tat showed no effect on the serum calcium level, which confirmed the hypocalcemic enhancing activity of the mixture which was from sCT/Tat mixture. For VP/sCT mixtures, no hypocalcemic effect was observed. This might be due to the lack of PVR in rat resulting from the rapid change of the PVR gene during evolution. Also, the rodent species were not susceptible to PV due to the low amino acid sequence similarity of rodent PVR to human PVR (Ida-

Hosonuma et al., 2003). For VP/Tat/sCT mixture, hypocalcemic activity could be observed 4 hr after oral administration of the mixture and the hypocalcemic activity was persisted until 12 hr after administration. The long-acting pattern of VP/Tat/sCT mixture might be also due to the slow release of sCT from the cage forming by hydrophobic residue of VP as indicated by FT-IR spectrum.

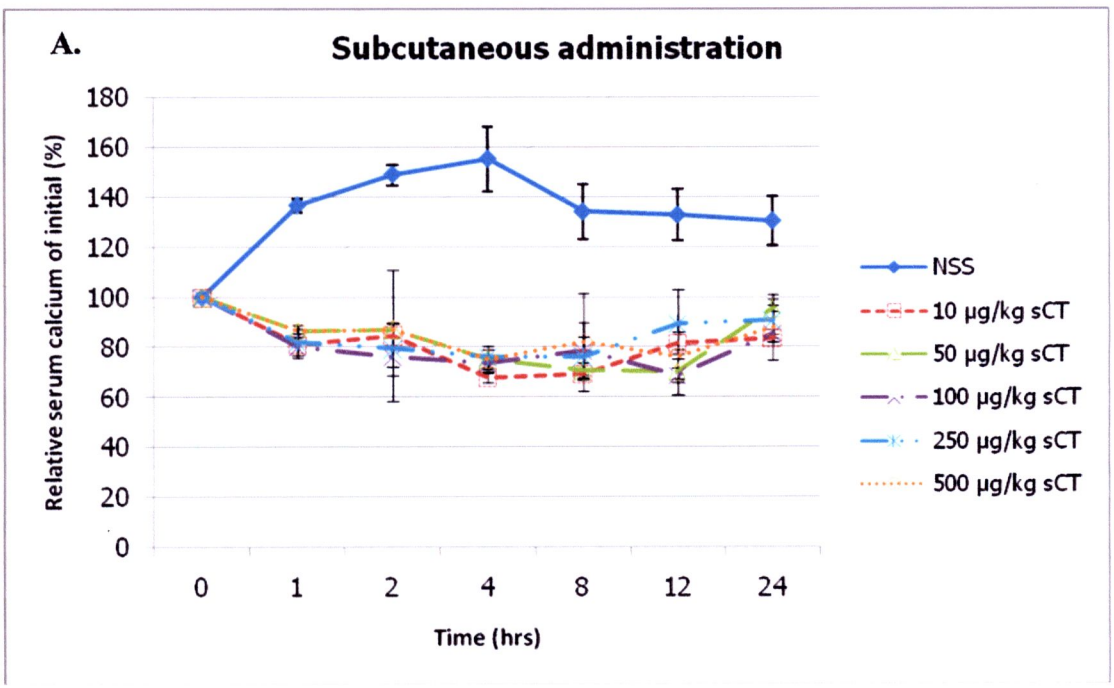

Figure 44 Relative serum calcium level in: **A.** Subcutaneous administration of sCT at various doses of 10, 50, 100, 250 and 500 µg/kg. **B.** Oral administration of sCT at the dose 50 µg/kg (300 IU/kg) or 3.64 µM, Tat at 32 µg/kg (3.64 µM), VP at 32 µg/kg (3.64 µM) and the mixtures containing sCT equivalent to 50 µg/kg

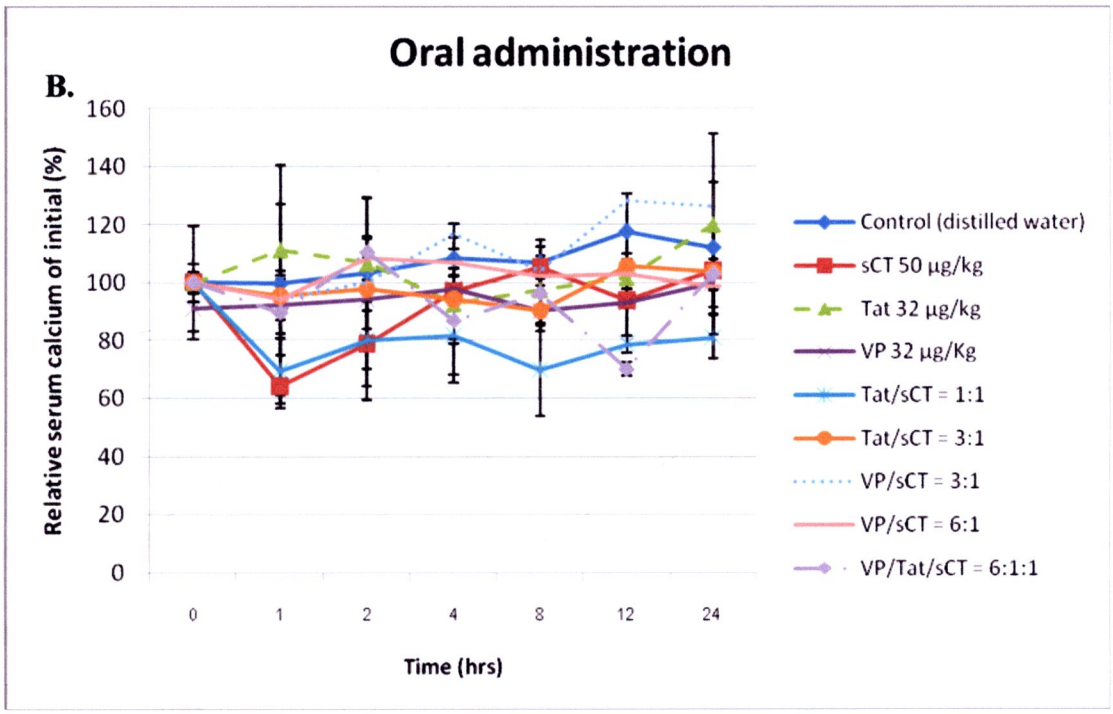

Figure 44 Relative serum calcium level in: **A.** Subcutaneous administration of sCT at various doses of 10, 50, 100, 250 and 500 µg/kg. **B.** Oral administration of sCT at the dose 50 µg/kg (300 IU/kg) or 3.64 µM, Tat at 32 µg/kg (3.64 µM), VP at 32 µg/kg (3.64 µM) and the mixtures containing sCT equivalent to 50 µg/kg (continued)

6.3. Transdermal absorption of sCT and Tat/sCT at 1:1 molar ratio

The enhancement of sCT transdermal absorption by co-incubation with Tat peptide was evaluated. Cumulative amounts (µg/cm^2) and fluxes (µg/cm^{2}hr) of sCT in VED and receiver compartment solution at 1, 3 and 6 hr were shown in Figure 45. The temperature in the receiving chamber which represented the systemic circulation was thermostated at 37°C according to the body core temperature which is about 37°C (Aizawa and Cabanac, 2000; Danet and Préat, 2003). Tat/sCT mixture gave the higher cumulative amounts and fluxes in both VED and receiver compartment than

sCT solution at all time point with the cumulative amounts in VED at 1, 3 and 6 hr of 0.67±0.18, 0.33±0.17 and 0.26±0.04 μg/cm^2, respectively and fluxes value in VED at 1, 3 and 6 hr of 0.67±0.18, 0.11±0.05 and 0.04±0.01 μg/cm^{2}hr, respectively. This might be due to the presences of positive-charged arginine groups in Tat which could enhances the binding of peptide complexes to negatively charged cell surfaces by electrostatic interactions (Fawell et al., 1994; Tseng et al., 2002). The importance of positive surface charges for the effective transdermal delivery for the electrostatic interaction with the skin barrier has been reported (Kim et al., 2010). It is known that the intercellular lipid domain of SC is different than any other cellular membrane by means of lipid composition, lipid/protein ratio and water content. The interaction of CPPs with lipids may be the main transport across SC as this interaction may destabilize SC resulting in an increase in the membrane permeability. Another mechanism of transport is suggested through the tight junctions of the skin. CPPs are proposed to disrupt these junctions and allow penetration into the viable skin layers (Lopes et al. 2008). Macropinocytosis is another possible transport pathway for the CPPs into mammalian cells. The cellular entry and transdermal delivery of CPPs has been shown to involve the macropinocytosis and actin reorganization (Hou et al. 2007). sCT from Tat-sCT mixture could be detected in receiver compartment at all time point with the cumulative amounts at 1, 3 and 6 hr of 0.20±0.08, 0.43±0.07 and 0.59±0.22 μg/cm^2, respectively and fluxes value at 1, 3 and 6 hr of 0.20±0.08, 0.14±0.02 and 0.09±0.04 μg/cm^{2}hr, respectively, while sCT from sCT solution could be detected in receiver compartment only at 6 hr. The amount of sCT detected in receiver compartment was gradually increased which was related to the decreased of sCT amount in VED. The active transport across lipid cellular membrane has been

reported as the mechanism of transport of CPPs-cargoes into the cutaneous barrier and demonstrated that the conjugates penetrate intact into the skin (Rothbard et al., 2000). Thus, CPPs-cargoes enter the layers of cells and get accumulated there, and then enter the adjacent layers presumably by forming a gradient. As known, the amount of sample detected in receiving chamber represented the possibility of sample to cross the skin barrier to circulation after transdermal application (Amsden and Goosen, 2004). Then, the physical mixing of Tat with targeted peptide might be applicable for the development of transdermal delivery system.

Percentages of sCT penetrated into VED and receiver compartment of each sample were shown in Figure 46. Without co-incubation with Tat peptide, 16.65±2.15% of sCT in solution could penetrate through excised rat skin at 6 hr. It has been reported that the truncated CT (amino acid 9-32) could be used as the carrier peptide. The truncated CT fragment was shown to internalize in several different cell lines in a concentration-, temperature- and time-dependent manner. Co-localization approaches, ATP depletion as well as competition studies strongly supposed a receptor-independent, endocytotic uptake (Rennert et al., 2008). However, the percentage of sCT penetrate through excised rat skin to the receiver compartment at 6 hr was increased to 58.36±21.34% in Tat/sCT mixture which was 3.50 times of sCT solution. These indicated the enhancement of sCT permeation through rat skin by Tat peptide.

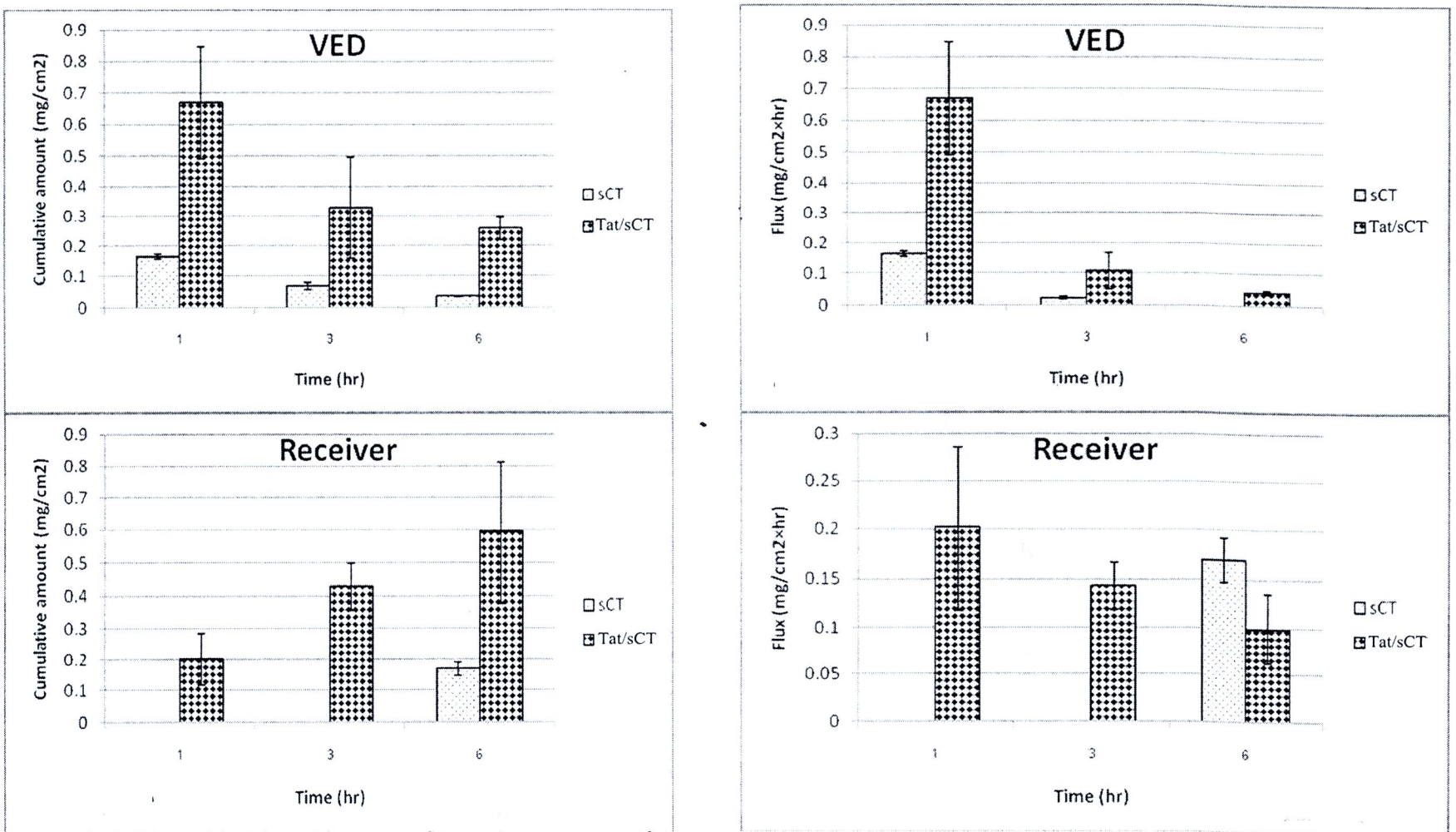

Figure 45 Cumulative amounts (μg/cm^2) and fluxes (μg/cm^{2}hr) of sCT of each sample in VED and receiver compartment solution at 1, 3 and 6 hour

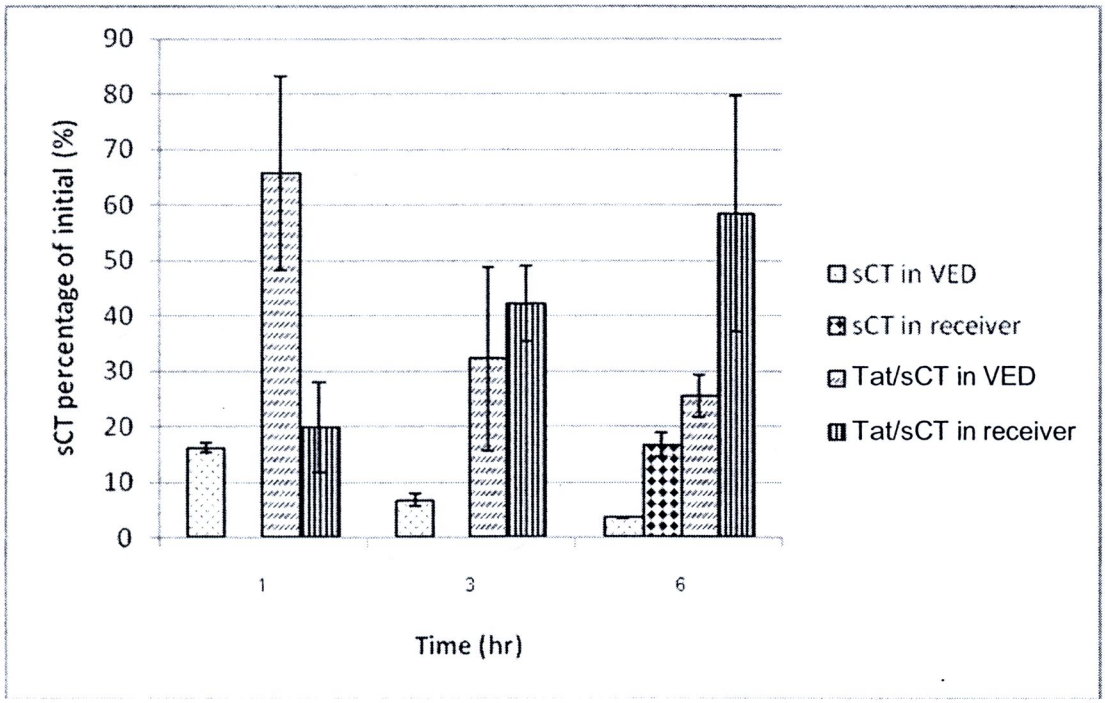

Figure 46 Percentages of sCT (%) detected in each compartment at various time intervals calculated from the initial sCT concentration in the sample (2.5 mg/ml)

6.4. Chemical stability of sCT and Tat/sCT mixture

Percentage remaining of sCT in sCT solution and Tat/sCT mixture after 1 month storage at 4±2 °C, room temperature (27±2 °C) and 45±2 °C was shown in Table 16. sCT solution showed good stability at 4°C with the percentage remaining of sCT at 1 month of 65.16%, while the remained sCT was under detection limit after kept at RT and 45°C for 1 month. Tat/sCT mixture demonstrated superior sCT stability than the sCT solution with sCT percentage remaining after 1 month storage at 4°C, RT and 45°C of 77.07, 71.55 and 52.94%, respectively. The hydrolytic degradation of CT in aqueous solution has been reported. CT undergoes deamidation at Gln14 and Gln20, backbone cleavage between Cys1 and Ser2,

oxidation of Cys1 or Cys7 followed by cleavage of the disulfide bond, formation of a trisulfide bond, isomerization at Pro23 and formation of reducible and non-reducible dimers at pH>3.3 (Stevenson and Tan, 2000). The thermal instability of CT has also reported by thermal FT-IR microspectroscopic evidences that after incubation at the accelerated temperature of 40°C, sCT structure would be transformed from predominant α-helix/random coil to β-sheet structure. The intramolecular and intermolecular β-sheet structures play an important role in the secondary conformational structure of sCT in the liquid state which exhibited the protein instability (Lee et al., 2009). However, the complex formation between sCT and Tat could provide the protective effect from hydrolytic and thermal degradation indicated by the higher percentage remaining of sCT at all storage temperature (Woods and Huestis, 2001).

Table 16 Percentage remaining of sCT in sCT solution and Tat/sCT mixture after 1 month storage at different temperatures

Sample	**Storage temperature**	**Percentage remaining**		
		1 wk	**2 wk**	**4 wk**
sCT	4°C	87.29%	69.90%	65.16%
	RT	81.45%	8.35%	ND
	45°C	72.97%	3.71%	ND
Tat/sCT	4°C	94.07%	81.47%	77.07%
	RT	88.74%	88.33%	71.55%
	45°C	67.07%	65.13%	52.94%